AUTHOR(S): TEBOWEI, R., HOSSAIN, M., ISLAM, S.Z., DROUBI, M.G. and OLUYEMI, G.

TITLE: Investigation of sand transport in an undulated pipe using computational fluid dynamics.

YEAR: 2018

Publisher citation: TEBOWEI, R., HOSSAIN, M., ISLAM, S.Z., DROUBI, M.G. and OLUYEMI, G. 2018. Investigation of sand transport in an undulated pipe using computational fluid dynamics. Journal of petroleum science and engineering [online], 162, pages 747-762. Available from: https://doi.org/10.1016/j.petrol.2017.11.003

OpenAIR citation: TEBOWEI, R., HOSSAIN, M., ISLAM, S.Z., DROUBI, M.G. and OLUYEMI, G. 2018. Investigation of sand transport in an undulated pipe using computational fluid dynamics. Journal of petroleum science and engineering, 162, pages 747-762. Held on OpenAIR [online]. Available from: https://openair.rgu.ac.uk

Accepted Manuscript

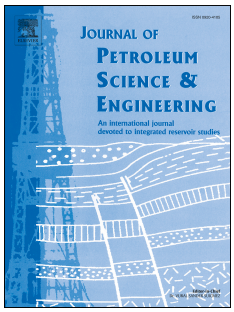

Investigation of sand transport in an undulated pipe using computational fluid dynamics

Roland Tebowei, Mamdud Hossain, Sheikh Zahidul Islam, Mohamad Ghazi Droubi, Gbenga Oluyemi

PII: S0920-4105(17)30886-0

DOI: 10.1016/j.petrol.2017.11.003

Reference: PETROL 4419

To appear in: *Journal of Petroleum Science and Engineering*

Received Date: 20 April 2017

Revised Date: 25 August 2017

Accepted Date: 2 November 2017

Please cite this article as: Tebowei, R., Hossain, M., Islam, S.Z., Droubi, M.G., Oluyemi, G., Investigation of sand transport in an undulated pipe using computational fluid dynamics, *Journal of Petroleum Science and Engineering* (2017), doi: 10.1016/j.petrol.2017.11.003.

Investigation of Sand Transport in an Undulated Pipe using Computational Fluid Dynamics

Roland Tebowei, Mamdud Hossain*, Sheikh Zahidul Islam, Mohamad Ghazi Droubi and Gbenga Oluyemi

School of Engineering, Robert Gordon University, Sir Ian Wood Building, Garthdee Road, Aberdeen, AB10 7GJ, UK

*Corresponding Author. Email: M.Hossain@rgu.ac.uk, Phone: +44 (0)1224 262351, Fax: +44 (0)1224 262444

Abstract

A CFD model has been implemented to investigate the effects the pipe undulation on sand transport. Of particular interest of the present study is the sand deposition in small angled V-inclined bend relevant to oil and gas subsea flowlines where sand deposition could be a major problem. The model used is the two-fluid Eulerian-Eulerian model with the granular temperature to tackle the solid phase properties. A number of sub-models for tackling solid-fluid and fluid-fluid interaction has been incorporated in the modelling frame work to capture the transition of flow regimes. The simulation results show that the seemingly small angled V-inclined has significant impact on sand disposition compared to the horizontal section. Sand is deposited at the downstream section of the V-inclined pipe at much higher velocities compared to the minimum transport velocity of the horizontal pipe.

Keywords: sand deposition; Eulerian model; V-inclined.

1. Introduction

The recent studies by Dabirian, Mohan and Shoham [1], Spillane and Leggoe [2], Bello, Oyeneyin and Oluyemi [3] and Zhu et al. [4] have reported that most of the prolific reservoirs with hydrocarbon reserve in commercial quantity worldwide are mainly formed of unconsolidated sandstone formations and are prone to produce sand with the hydrocarbon fluids. Therefore, petroleum multiphase pipelines would generally contain a flow-stream of liquid, gas and solid particles (sand) phases or mainly liquid and sand for hydrocarbons with very low gas-oil ratio. The knowledge of the nature of the sand particles interaction with the fluids and movements in pipelines is imperative, in order to understand the implications of sand particles transport in hydrocarbon flow stream in pipelines. The presence of sand particles in hydrocarbon flow-stream is a major risk factor to pipe blockage that may lead to reduced oil-well performance which increases work-over frequency [5]. Sand deposition may occur in pipelines due to changes in flow conditions, which may include flow-rates and pipe inclination, to mention a few. The sand deposit may cause flow impediment, erosion and corrosion of pipes, and other flow assurance issues. These problems due to produced sand may occur more often in offshore subsea pipelines, which are usually route through undulating seabed topology [6]. The undulating nature of seabed terrain causes pipe bend (pipe-dip) sections in long subsea pipelines route through seabed to production platform. The dip points are

generally known as low-points of pipelines where stationary solids bed may accumulate and the likely spot where pipe leaks may occur [7-9]. Stationary sand deposit in pipe and pipe bend sections may result in additional pressure loss in pipelines, which may eventually impede production and consequently result in economic risks [10]. Therefore, it is vital to ensure multiphase pipelines are designed and operated such that transport of sand particles can be managed to avoid stationary sand deposit and abrasion of pipes in order to ensure oil and gas flow assurance. Therefore, a robust understanding of the hydrodynamics mechanisms which play critical roles in the transport of solids in pipelines is imperative, in order to provide accurate guidance to optimize pipe design for efficient sand management.

The characteristics of sand transport in pipelines may be described by flow regime, which represents the distribution pattern of the sand-phase in the fluid phase. From hydrodynamics perspective, at a sufficiently high flow velocity, the sand-phase may be fully suspended in the carrier fluid, this phenomenon is known as homogeneous flow regime [11]. However, if the flow velocity reduces to a certain threshold, the sand may segregate towards the pipe-bottom and transported as heterogeneous flow pattern. At a much reduced velocity, the heterogeneous flow may further result in moving sand bed flow regime and eventually formation of a stationary sand deposit in pipes [12]. Several studies have been carried out by researchers such as Bello et al. [3], Salama [13], Danielson [8], Oudeman [12] and Doron and Barnea [14], in order to determine the critical conditions for various sand flow regimes pipe, particularly the velocity leading to stationary sand deposit in pipes. However, most of the studies

focused on flow in horizontal and other forms of inclined pipes with little or no attention given to flow in V-inclined. The pipe bend angles considered in the few studies by Osho et al. [15] and Yan et al. [16] and King et al. [17] that investigated flow in V-inclined bend pipes, do not represent a typical gradient of offshore seabed undulation dip. The typical gradient of seabed topology is formed of undulations of approximately $1-6^{o}$ upward and downward slope angles [18].

A matter of practical importance in the oil industry is predicting multiphase flow phenomena in pipeline systems of various inclinations such as the V-inclined pipe bend of the seemingly small bend angles. There exist several predictive correlations for predicting critical sand transport velocity in pipes. However, correlations are mostly valid for the particular type of system producing the data in which the correlation has been developed. In practise, generic application of the existing correlations has often led to erroneous prediction of flow regimes, pressure drop or minimum transport velocity (MTV) [6]. This drawback necessitates the need for more investigations for sand transport flow in pipe bends of angles that represent a typical gradient of seabed topology in order to improve the accuracy of predictions for sand transport phenomena in subsea multiphase pipelines.

The subsea pipelines (flowlines) unavoidably follow the seabed hilly terrain, which comprises of horizontal, slightly downhill and uphill landscape [19]. Therefore, majority of pipelines installed on the seabed are always undulated at various shallow angles caused by seabed

topology [17]. Consequently, in addition to the spatial distribution of gas-liquid flow regime issues which complicate predictions of sand settling in petroleum flowlines, the abrupt change in subsea pipeline inclination due to shallow pipe-dip adds to the complex nature of multiphase flow dynamics in the pipeline and in turn add to the difficulty in predicting sand settling in subsea pipelines. Understanding the flow mechanisms of multiphase mixture through pipe bends (dip) may play a crucial role in the economic transport of hydrocarbon fluids in pipelines. However, the flow in pipe bends of subsea undulating pipelines are seldom reported in literature compared to flow in horizontal and other forms of inclined pipes, due to the complexity of flow in pipe bends [20].

The studies by Huang et al. [20], Al-Safran et al. [21], Issa and Kwemf [22], Taitel et al [23] have investigated flow in hilly terrain pipes, in which shallow angle pipe bend (dip) section exists. However, the studies focused on liquid-gas flow without solids phase. The majority of the studies reported that the flow characteristics of liquid and gas at the dip of V-inclined pipe bend is coupled by those of the downhill and uphill sections of the pipe bend. Issa and Kwemf [22] investigated liquid-gas flow in horizontal, downward inclined and shallow V-inclined pipes, and reported that slug initiation mechanism in the V-inclined pipe downhill section is different from that in the uphill section of the pipe. They mentioned that the slugging in the horizontal and -1.5^{o} downward inclined pipes was initiated by hydrodynamics instability, whereas the slug in the V-inclined pipe was initiated by both hydrodynamics instability and terrain induced due to the pipe curvature effect. Although, solids phase is not included in

the gas-liquid flow investigated by Issa and Kwemf [22], but the slug initiation mechanism in the $\pm 1.5^{o}$ V-inclined pipe suggests that the pipe curvature of the seemingly shallow angle pipe bend influenced the multiphase flow characteristics in modes which are not observed in the horizontal and -1.5^{o} downward inclined pipes. The pipe curvature effect on slug initiation mechanisms in the V-inclined pipe may also play a crucial role in sand transport characteristics in V-inclined pipe bends.

The literature is limited in studies on sand transport in shallow angle multiphase inclined pipes that represent the typical inclined pipe sections of subsea petroleum flowlines. Critical review of the available literature shows that majority of the studies which studied sand transport in low angle inclined pipes focused on a standalone section of the low angle downward inclined pipe or upward inclined pipes separately, and reported contrast findings of effects of the low angle inclined pipes on sand transport characteristics. The previous study by Al-lababidi et al [10] reported that the characteristics of sand-liquid transport in horizontal and $+5^{o}$ upward inclined pipe are similar. However, the more recent study by Goharzadeh et al. [24] found that the transport characteristics of moving sand bed and sand dunes in +1 upward inclined pipe is different and more complex compared to that in horizontal pipe.

The study by Danielson [8] investigated sand transport in liquid and liquid-gas flow in -1.35 and +4 upward inclined pipes concluded that the pipe inclinations do not have effect on sand transport in liquid, except for gas-liquid flows. Conversely, the experimental study by Nossair et al. [25] of

sand-liquid transport in +3.6° upwind inclined pipe showed that higher flow rate is required to move stationary sand deposit in the seemingly small angle upward inclined pipe compared to a horizontal pipe. Stevenson and Thorpe [26] also reported that downward inclined flowlines are more susceptible to sand deposition than upward inclined flowlines. This disparity in the findings reported by various author in the literature shows that sand transport characteristics in low angle inclined pipe is yet not well understood.

In addition to the disparity in reports by previous researchers on effect of low angle inclined pipes on sand transport characteristics in pipes, the investigation approach in which sand transport is investigated by flow in standalone downward and upward inclined pipe sections may not reveal the actual complexity of sand transport characteristics in V-inclined undulated pipe. This may be a reason for the assumption by previous researchers that shallow angle inclined petroleum flowline bends (pipe dips) do not have effect on sand transport characteristic and critical sand transport velocity in pipes. Consequently, there is paucity of published research studies on sand transport in shallow angle V-inclined pipe bends. The only available published studies on sand transport in multiphase bend pipes that represent the seemingly small gradient V-inclined pipe bend are the experimental studies by Kings et al. [17] and Tippet and Priestman [18].

Although, Yan et al. [16] also studied sand transport in pipe bend, but the curvature angle of ±24° of the V-inclined pipe investigated seems inordinate

pipe curvature for a typical seabed undulation. Tippet and Priestman [18] have previously pointed out that the typical gradient of seabed undulation is approximately $\pm$1-6^{o} and the results from their study show that pipe bends of such seemingly small gradient have significant effects on sand mobility in pipes. The more recent study on sand transport in pipe bend by Kesena et al. [27] focused on sand transport in pipe-elbow, which gives a good representative of bend pipes at the riser junction between subsea flowlines and riser systems, but not for flowline dips.

The effect of the seemingly small gradient $\pm$1-6^{o} V-inclined pipe bend that represent subsea flowline-dips on sand mobility as reported in the few available studies implies that flowline-dips may have effect on critical or minimum sand transport velocity differently from those of other inclined pipes. However, to the best of the knowledge of the present study, there is no existing published minimum transport velocity (MTV) correlation for predicting sand settling in V-inclined multiphase pipes. Therefore, more work is required on sand transport in multiphase flowlines which take into account the local sand concentration distribution and other hydrodynamics parameters of liquid-sand flow in V-inclined pipes in order to improve the understanding of sand transport in subsea multiphase flowlines and to develop correlation for predicting sand settling in multiphase flowline-dips.

Therefore, the purpose of this study is to implement a three-dimensional (3D) CFD model framework that accounts for the interactions between liquid-particle, particle-particle and pipe wall and numerically simulate sand transport characteristics and sand deposition in V-inclined bend pipe

using particle parameters that represent the produced sand in petroleum production. The numerical investigation will provide improved understanding of sand transport characteristics in petroleum flowline-dips and predictions of the minimum transport velocity for sand suspension and stationary sand deposit regimes in pipe dips based on accurate knowledge of the local sand concentration distribution in the pipe. Correlations developed based on accurate knowledge of local sand concentration distribution in liquid is essential in order to improve the predictions of sand settling in gas-liquid-sand three-phase flow in multiphase bend pipes. The CFD approach if appropriately tuned offers the advantage of providing more detailed and accurate information of the local flow parameters rapidly which may be difficult to obtain experimentally. The present study treats solid water slurry flow at a continuum level treating as two different fluids. Inclusion of rheological properties of slurry as published in [28-29] could further improve the results.

2. Mathematical Model

In the present study, the Eulerian-Eulerian two-fluid model has been utilised to simulate the sand transport in pipelines. The key feature of the Eulerian-Eulerian model is the solution of separate transport equations for each phases. The main challenge in Eulerian-Eulerian model comes from selecting appropriate sub-models that account for the complex

interactions between fluid-solid and solid-solid from dilute to dense sand concentrations.

2.1 Momentum Equations:

The Eulerian-Eulerian model solves a number of constitutive equations as given below:

Continuity equation:

$$\nabla.(\alpha_t \rho_t \vec{v}_t) = 0 \quad (1)$$

Where, $t = s, f$ and s stands for solid and f for fluid.

Momentum equation:

Two individual momentum equations are solved for fluid and solid phases as below:

For fluid:

$$\nabla.\left(\alpha_f \rho_f \vec{v}_f \vec{v}_f\right) = -\alpha_f \nabla P + \nabla.\left(\bar{\bar{\tau}}_f + \bar{\bar{\tau}}_{t,f}\right) + \alpha_f \rho_f g + K_{sf}\left(\vec{v}_s - \vec{v}_f\right) \quad (2)$$

For solid:

$$\nabla.(\alpha_s \rho_s \vec{v}_s \vec{v}_s) = -\alpha_s \nabla P - \nabla P_s + \nabla.\left(\bar{\bar{\tau}}_s + \bar{\bar{\tau}}_{\tau,f}\right) + \alpha_s \rho_s g + K_{fs}(\vec{v}_f - \vec{v}_s) \quad (3)$$

Where, $\vec{\tau}_{t,f}$ is Reynold stress tensor and the method of calculating this is explained later.

$\bar{\bar{\tau}}_s$, $\bar{\bar{\tau}}_f$ are viscous stress tensor for solid and fluid respectively, which are expressed as:

$$\bar{\bar{\tau}}_s = \alpha_s \mu_s (\nabla \vec{v}_s + \nabla \vec{v}_s^{tr}) + \alpha_s \left(\lambda_s - \frac{2}{3}\mu_s\right) \vec{\nabla}.\vec{v} \bar{\bar{I}} \quad (4)$$

And, $\bar{\bar{\tau}}_f = \alpha_f \mu_f \left(\nabla \vec{v}_f + \nabla \vec{v}_f^{tr}\right)$ (5)

Where, with the superscript "tr" over velocity indicates transpose and $\bar{\bar{I}}$ is the identity vector.

λ_s is the bulk viscosity of solid, which is defined according to Lun et al [28] as:

$$\lambda_s = \frac{4}{3}\alpha_s \rho_s d_s g_{o,ss}(1 + e_{ss}) \left(\frac{\Theta_s}{\pi}\right)^{\frac{1}{2}} \quad (6)$$

Where, d_s is the solid particle diameter.

$g_{o,ss}$ is the radial distribution function, which indicates the probability of the particle-particle contact. The expression for the radial distribution function used in the present study is proposed by Lun et al [30]:

$$g_{o,ss} = \left[1 - \left(\frac{\alpha_s}{\alpha_{s,max}}\right)^{\frac{1}{3}}\right]^{-1} \quad (7)$$

Where, $\alpha_{s,max}$ is the maximum packing density and for the mono-dispersed sphere particles, this value has been taken as 0.63. e_{ss} is the co-efficient of restitution and is taken as 0.9. Θ_s is the granular temperature, which represents the kinetic energy of fluctuating particle motion.

μ_f is the shear viscosity of the fluid and μ_s is the shear viscosity of solids defined as:

$$\mu_s = \mu_{s,col} + \mu_{s,kin} + \mu_{s,fr} \quad (8)$$

Where, $\mu_{s,col}$ represents the solid viscosity due to collisions, $\mu_{s,kin}$ is the solid viscosity due to kinetic fluctuations of solid particles and $\mu_{,fr}$ is the solid viscosity representing particle-particle contact. The collisional viscosity was calculated using Gidaspow et al [31], the kinematic viscosity using Syamlal et al [32] and the frictional viscosity using Schaeffer [33]:

$$\mu_{s,col} = \frac{4}{5}\alpha_s \rho_s d_s g_{o,ss}(1 + e_{ss})\left(\frac{\Theta_s}{\pi}\right)^{\frac{1}{2}} \quad (9)$$

$$\mu_{s,kin} = \frac{\alpha_s \rho_s d_s \sqrt{\Theta_s \pi}}{6(3 - e_{ss})}\left[1 + \frac{2}{5}(1 + e_{ss})(3e_{ss} - 1)\alpha_s g_{o,ss}\right] \quad (10)$$

$$\mu_{s,fr} = \frac{P_s \sin(\phi)}{2\sqrt{I_{2D}}} \quad (11)$$

Where, I_{2D} is the second invariant of the deviatoric strain rate tensor for solid phase and P_s is the solid pressure given as,

$$P_s = \alpha_s \rho_s \Theta_s + 2\rho_s(1+e_{ss})\alpha_s^2 g_{o,ss}\Theta_s \quad (12)$$

and ϕ is internal friction angle taken as 30^O in the present study.

When the volume fraction of solid particles tend to reach the packing limits, the solid pressure is dominated by particle friction. Thus Johnson and Jackson [34] model has been included in the solid pressure calculation as:

$$P_{fric} = Fr\frac{(\alpha_s - \alpha_{s,min})^n}{(\alpha_{s,min} - \alpha_s)^p} \quad (13)$$

Where, $Fr = 0.05$, $n = 2$ and $p = 5$. The critical value for the solid volume fraction is $\alpha_{s,min} = 0.5$.

K_{sf} or K_{fs} is the interphasial momentum exchange co-efficient given by,

$$K_{sf} = K_{fs} = \frac{3}{4}\frac{\alpha_s \alpha_f \rho_f}{V_{r,s}^2 d_s} C_D \left(\frac{Re_s}{V_{r,s}}\right)\left|\vec{v}_s - \vec{v}_f\right| \quad (14)$$

Where, the drag co-efficient C_D is given by [35],

$$C_D = \left[0.63 + 4.8\left(\frac{Re_s}{V_{r,s}}\right)^{-\frac{1}{2}}\right]^2 \quad (15)$$

Re_s is the relative Reynolds number between phases 'f' and 's' given by,

$$Re_s = \frac{\rho_f d_s |\vec{v}_s - \vec{v}_f|}{\mu_f} \quad (16)$$

$V_{r,s}$ is the terminal velocity correlation for solid phase given by [35],

$$V_{r,s} = 0.5\left(A - 0.06Re_s + \sqrt{(\{(0.6Re_s)^2 + 0.12Re_s(2B - A) + A^2\}}\right) \quad (17)$$

Where, $A = \alpha_f^{4.14}$; $B = 0.8\alpha_f^{1.28}$ for $\alpha_f \leq 0.85$ (18)

$A = \alpha_f^{4.14}$; $B = \alpha_f^{2.65}$ for $\alpha_f > 0.85$

2.1.1 Turbulent dispersion force

Interphase turbulent momentum transfer can be included through the turbulent dispersion force added as a source term in the momentum equations. The turbulence dispersion force is defined as:

$$\vec{F}_{td,s} = -\vec{F}_{td,f} = -K_{sf}\vec{v}_{dr} \quad (19)$$

Where, $\vec{v}_{dr}$ is the drift velocity and it represents the dispersion of the secondary phases due to the turbulent fluid motion. $\vec{v}_{dr}$ is calculated as,

$$v_{dr} = -D_{fs}\left(\frac{\nabla\alpha_f}{\alpha_f} - \frac{\nabla\alpha_s}{\alpha_s}\right) \quad (20)$$

Where D_{fs} is the fluid-particle dispersion tensor.

2.2 Turbulence Model

There are several ways to treat turbulence effects such as $k-\epsilon$ mixture turbulence model [36] and a dispersed turbulence model [37]. In the present study, the dispersed turbulent model has been used in order to handle the ranges of sand transport flow regime from immobile bed to full suspended flow based on the authors' work [38]. While, the $k-\epsilon$ mixture turbulence model may be a good option for fully suspended flow to reduce computational overhead [38].

2.1.1 The $k-\epsilon$ Dispersed Turbulence Model

In this model formulation, the random motion of particle phase influences the fluid phase turbulence. The fluctuating quantities for the secondary phase is quantified using mean flow characteristics of the primary phase, the particle relaxation time and the eddy-particle interaction time.

The turbulence for fluid phase is governed by the standard $k-\epsilon$ model with the effects of solid-fluid interactions are accounted for through different source terms.

Reynolds stress tensor for the fluid phase is,

$$\bar{\bar{\tau}}_{t,f} = -\frac{2}{3}\left(\rho_f k_f + \rho_f \mu_{t,f} \nabla \vec{u}_f\right)\bar{\bar{I}} + \rho_f \mu_{t,f}\left(\nabla \vec{u}_f + \nabla \vec{u}_f^{tr}\right) \quad (21)$$

Where, $\mu_{t,f}$ is the turbulent viscosity is given by,

$$\mu_{t,f} = \rho_f C_\mu \frac{k_f^2}{\epsilon_f} \text{ with } C_\mu = 0.09 \quad (22)$$

The predictions of turbulent kinetic energy k_f and its rate of dissipation ϵ_f are obtained from the following transport equations,

Turbulence kinetic energy, k_f:

$$\nabla.\left(\alpha_f \rho_f \vec{v}_f k_f\right) = \nabla.\left(\alpha_f \frac{\mu_{t,f}}{\sigma_k} \nabla k_f\right) + \alpha_f G_{k,f} - \alpha_f \rho_f \epsilon_f + \alpha_f \rho_f \prod_{kf} \quad (23)$$

Energy dissipation rate, ϵ_f :

$$\nabla.\left(\alpha_f \rho_f \vec{v}_f \epsilon_f\right) = \nabla.\left(\alpha_f \frac{\mu_{t,f}}{\sigma_\epsilon} \nabla \epsilon_f\right) + \alpha_f \frac{\epsilon_f}{k_f}\left(C_{1\epsilon} G_{k,f} - C_{2\epsilon} \rho_f \epsilon_f\right) + \alpha_f \rho_f \prod_{\epsilon_f} \quad (24)$$

Where, $\prod_{kf}$ and $\prod_{\epsilon f}$ represent the influence of the solid phase 's' on the fluid phase 'f' given by,

$$\prod_{kf} = \frac{K_{fs}}{\alpha_f \rho_f}\left(k_{sf} - 2k_f + \vec{v}_{sf}.\vec{v}_{dr}\right) \quad (25)$$

$$\prod_{\epsilon,f} = C_{3\epsilon} \frac{\epsilon_f}{k_f} \prod_{kf} \quad (26)$$

$\vec{v}_{dr}$ is the drift velocity given by,

$$\vec{v}_{dr} = \left(\frac{D_s}{\sigma_s \alpha_s}\nabla\alpha_s - \frac{\mu_{t,f}}{\sigma_{sf}\alpha_f}\nabla\alpha_f\right) \quad (27)$$

Where, $\nabla\alpha_s$ accounts for the concentration fluctuations. v_{sf} is the slip velocity, the relative velocity between fluid phase and solid phase given by,

$$\vec{v}_{sf} = \vec{v}_s - \vec{v}_f \quad (28)$$

D_s is the eddy viscosity of the solid phase defined in the next section. σ_{sf} is a constant taken as 0.75. k_{sf} is the co-variance of the velocity of fluid and solid phase. It represents the product of fluid and solid phase velocity fluctuations. $G_{k,f}$ is the generation of turbulent kinetic energy in the fluid field defined as:

$$G_{k,f} = \mu_{t,f}\left(\nabla\vec{v}_f + \nabla\vec{v}_f^{\,t}\right):\nabla\vec{v}_f \quad (29)$$

The turbulent model constants are:

$C_{1\epsilon} = 1.44$, $C_{2\epsilon} = 1.92$, $C_{3\epsilon} = 1.20$, $\sigma_k = 1.0$, $\sigma_\epsilon = 1.3$

Turbulence model closure for the solid phase:

Turbulence in the solid phase is represented by Tchen Theory which calculates the dispersion of discrete particles in homogeneous and steady turbulent field.

The time scale considering inertial effects acting on a solid particle:

$$\tau_{F,sf} = \alpha_s \rho_f K_{sf}^{-1} \left(\frac{\rho_f}{\rho_s} + C_{vm} \right) \tag{30}$$

The characteristic time scale of eddy – particle interaction:

$$\tau_{t,sf} = \tau_{t,f} \left[1 + C_\beta \xi^2 \right]^{-\frac{1}{2}} \tag{31}$$

$$\xi = \frac{|\vec{V}_r|}{\sqrt{\frac{2}{3} k_f}} \tag{32}$$

The characteristic time of energetic turbulent eddies,

$$\tau_{t,f} = \frac{3}{2} C_\mu \frac{k_f}{\epsilon_f} \tag{33}$$

V_r is the local relative velocity between particle and surrounding fluid defined as the difference between the slip and drift velocity:

$$|V_r| = \vec{v}_{sf} - \vec{v}_{dr} \tag{34}$$

$$C_\beta = 1.8 - 1.35\cos^2\theta \quad (35)$$

θ is the angle between the mean particle velocity and the mean relative velocity.

η_{sf} is the ratio of two characteristics time:

$$\eta_{sf} = \frac{\tau_{t,sf}}{\tau_{F,sf}} \quad (36)$$

k_s is the turbulent kinetic energy of solid phase:

$$k_s = k_f\left(\frac{b^2+\eta_{sf}}{1+\eta_{sf}}\right) \quad (37)$$

$$k_{sf} = 2k_s\left(\frac{b+\eta_{sf}}{1+\eta_{sf}}\right) \quad (38)$$

The eddy viscosity of the solid phase is then calculated as:

$$D_s = D_{t,sf} + \left(\frac{2}{3}k_s - b\frac{1}{3}k_{sf}\right)\tau_{F,sf} \quad (39)$$

Where, $D_{t,sf}$ is the binary turbulent diffusion coefficient and is given by:

$$D_{t,sf} = \frac{1}{3}k_{sf}\,\tau_{t,sf} \quad (40)$$

and, $b = (1 + C_{vm})\left(\frac{\rho_s}{\rho_f} + C_{vm}\right)^{-1}$ (41)

2.3 Transport equation for granular temperature

The granular temperature for the solid phase represents the kinetic energy of the randomly fluctuated particles. It can be understood as the root mean square of grain velocity fluctuations and it provides and it is analogous to the thermodynamics temperature. The transport equation for the granular temperature is defined as:

$$\frac{3}{2}\nabla.(\rho_s\alpha_s\vec{v}_s\Theta_s) = \left(-P_s\bar{\bar{I}} + \bar{\bar{\tau}}_s\right):\nabla v_s + \nabla(k_{\Theta s}\nabla\Theta_s) - \gamma_{\Theta_s} + \Phi_{fs} \quad (42)$$

$k_{\Theta s}$ represents the diffusion coefficient and is defined as:

$$k_{\Theta_s} = \frac{15d_s\rho_s\sqrt{\Theta_s\pi}}{4(41-33\eta)}\left[1 + \frac{12}{5}\eta^2(4\eta-3)\alpha_s g_{o,ss} + \frac{16}{15\pi}(41-33\eta)\eta\alpha_s g_{o,ss}\right] \quad (43)$$

$$\eta = \frac{1}{2}(1+e_{ss}) \quad (44)$$

The energy dissipation rate of particles due to collisions among the particles is given by:

$$\gamma_{\Theta_s} = \frac{12\left(1-e_{ss}^2\right)g_{o,ss}}{d_s\sqrt{\pi}} \quad (45)$$

Φ_{fs} represents the transfer of the kinetic energy of random fluctuations in particle velocity from the solid phase 's' to the fluid phase 'f' and is given by:

$$\Phi_{fs} = -3K_{fs}\Theta_s \quad (46)$$

In the present study, an equilibrium model for the granular temperature has been utilised by neglecting the convection and diffusion term in Equation (43).

2.4 Solution Techniques

The governing continuity, momentum and turbulence equations have been solved using a finite volume technique. In the finite volume technique, momentum and turbulence equations have been discretised by the second-order upwind scheme, while the volume fraction equation by the first order upwind. The pressure and velocity equations are coupled using a phase coupled SIMPLE algorithm. The equations are solved in transient mode with a time step of 0.001s until a steady-state solution has been reached. The under-relaxation factor is also used to control the stability and convergence rate of numerical simulation. Appropriate values of under-relaxation factor in the range of 0.3-0.7 have been specified for pressure, momentum, turbulent kinetic energy and dissipation rate, and turbulent viscosity in the solver.

2.5 Description of pipe bend geometry and flow conditions

The schematic of the V-inclined pipe bend investigated in the present study is shown in Figure 1. The sections denoted P1, P2, P3 and P4 on the

bend pipe as shown in the figure are the pipe sections where the predicted data have been obtained for analysis. The pipe sections have been identified as the critical sections of the bend pipe where significant variations in sand deposit have been observed after a thorough visualization of the contour plots of sand concentration in the pipe across the range of flow velocities investigated. The section denoted P2 represents the pipe-dip and the other pipe sections P1, P3 and P4 are located at distance 10D, 2.5D and 15D away from the pipe dip, respectively, where D represents pipe diameter. The data obtained at sections P1, P3 and P4 represent the flow conditions at the upstream before entering the dip, dip-exit and further downstream of the dip, respectively.

Figure 2 presents the computational mesh structures of the $\pm 6^{o}$ and $\pm 4^{o}$ V-inclined pipe bend geometry. Table 1 presents the simulation conditions and the estimated minimum sand transport velocity (MTV) for an equivalent horizontal pipe flow. The MTV has been estimated from the Oroskar and Turian [39] MTV correlation.

3. Results and Discussion

The CFD model predictions have been extensively validated against the published experimental data for a range of solid transport flow regime and in a separate article by the authors [38]. The good agreement between the CFD model predictions and the experimental data shows that the treatment of the solids-phase turbulence kinetic energy in addition with the transport equation for the turbulence kinetic energy of the liquid

phase is essential for modelling the various liquid-solids transport flow regimes.

Figure 3 shows a comparison of the predicted sand concentration profiles at the pipe sections of the ±6° pipe bend for various flow velocities and sand particle size of 255μm. An asymmetric distribution of sand concentration across the pipe sections is displayed by the profiles and the particles segregated towards the pipe bottom at all the flow velocities. The sand concentration at the bottom-wall of all the pipe sections at 3.7 m/s is less than the concentration limit for loose-packed particles (Cv=0.5), beyond which particles may undergo enduring contact with each other. The MTV estimated for sand transport in an equivalent horizontal pipe flow is 1.48 m/s ≈ 1.5 m/s, as presented in Table 1. It is observed that the concentration at the bottom of the sections P1, before the dip, P2, dip, and P4, downstream of the bend pipe exceeded the loose-packed particles limit well before the velocity approached the 1.5 m/s, MTV estimated for horizontal pipe flow. At the 1.5 m/s velocity, the concentration at the pipe bottom of all the pipe sections has exceeded the limit for loose-packed particles. The degree of sand stratification in the bend pipe varies at all the flow velocities as can be seen in Figure 3. The steepness of the profiles closest to the pipe bottom-wall $^{y}/_{D} \leq 0.05$ started to develop at 3 m/s at sections P1, P2 and P4, and developed into an appreciable thickness at sections P1 and P4 as the velocity reduced to 2.5 m/s. The thickness of the steepness of profiles at sections P1 and P4 developed to $^{y}/_{D} = 0.15$ at 1.5 m/s and became uniform at all the pipe sections at 1 m/s. The concentration at the pipe bottom and the degree of sand

stratification suggested several critical conditions in the pipe bend at certain velocities such as the 3 m/s and 2.5 m/s, in which the profiles steepness at the pipe bottom developed at certain sections of the pipe bend. Also, the 1.5 m/s and 1 m/s velocities in which the sand concentration at all the pipe sections exceeded the limit of loose-packed particles and the steepness of the profiles at the pipe bottom became uniform at all the pipe bend sections.

Figures 4 and 5 present contour plots of sand concentration and liquid velocity magnitude in the bend pipe sections with the equivalent horizontal pipe case at the 3 m/s and 2.5 m/s velocity, respectively, which are above the 1.5 m/s MTV estimated for the horizontal pipe flow. Qualitative observations of the contours in Figure 4 (b) show that the maximum point of the liquid-phase velocity magnitude is located close to the bottom of the bend pipe at section P3, which represents the pipe-dip exit, while those of the other bend pipe sections and the horizontal pipe are in the pipes centre region. Also, the velocity magnitude is nearly uniform at section P3 compared to the other bend pipe sections and the horizontal pipe cross-section. The near uniformity of the velocity magnitude at section P4 diminished substantially in the pipe lower-half region towards the pipe bottom, whereas those of sections P1 and P2 are similar to that of the horizontal pipe. Consequently, the highest sand concentration is noticeable at the bottom of section P4 and the least concentration at section P3 where the velocity magnitude is nearly uniform, as can be seen when the contours in Figures 4 (a) and (b) are observed simultaneously.

The contours of sand concentration and velocity magnitude at 3 m/s in Figure 4 and those obtained at 2.5 m/s have similar trend, as shown in Figure 5. However, the thickness of the sand concentration at the pipe bottom at sections P1 and P4 at the 2.5 m/s velocity has substantially exceeded that of the equivalent horizontal pipe. The sand concentration at section P3 became more appreciable at 2.5 m/s compared to that at 3 m/s, as can be seen in Figures 5 (a) and 4 (a), respectively.

Figures 6 and 7 show the predicted contours of sand concentration and liquid-phase velocity magnitude in the bend pipe at 1.5 m/s and 1 m/s, which corresponds to the velocities at the MTV estimated for the horizontal pipe flow and below the estimated MTV, respectively. Figure 6 (b) shows that the velocity magnitude is nearly uniform at section P3 of the bend pipe at 1.5 m/s as previously observed in Figures 4 (b) and 5 (b) at the velocities above the MTV estimated for horizontal pipe flow. However, at 1 m/s the near-uniformity of the velocity magnitude at section 3 diminished significantly compared to those of the other pipe sections at the same velocity as can be seen in Figure 7 (b). Consequently, the highest sand concentration at the bend pipe bottom at the 1 m/s velocity is observed at section 3 compared to the other bend pipe sections and the horizontal pipe case.

Summarising the observations from the contour plots of Figures 4-7, it has been shown that the maximum sand concentration is located at section P4 and the least at section P3 at the velocities above the MTV estimated for

an equivalent horizontal pipe. However, at velocities below the MTV estimated for the horizontal pipe flow the maximum sand concentration is located at section P3 and the least at section P2.

Figure 8 shows the predicted profiles of the liquid-phase turbulence kinetic energy, in which the effect of the sand-phase on the multiphase turbulence has been accounted. The profiles are asymmetric at high velocities and then became gradually symmetric at certain pipe sections as the velocity varied from 3.7 m/s – 0.3 m/s. The figure shows that the turbulence intensity dissipated towards the bottom wall of the bend pipe, in the direction where the sand particles accumulated as the velocity reduced.

It can be seen in Figure 8 that at 3.7 m/s and 2.5 m/s the peak of turbulent kinetic is located at sections P3 and P4 in the pipe-core region ($0.3 < {}^{y}/_{D} < 0.8$), compared to sections P1 and P2. However, this trend shifted to the pipe lower-half region ${}^{y}/_{D} < 0.4$ as the velocity dropped below 2.5 m/s. Also, at the 3.7 m/s and 2.5 m/s, significant difference in turbulence intensity is observed between sections P2 and P3.

It can also be seen in Figure 8 that at the velocities below the estimated MTV of 1.5 m/s, all the profiles of turbulence intensity are similar in the pipe top half. However, in certain region of the pipe lower half, $0.1 < {}^{y}/_{D} < 0.3$, the profiles of sections P1 and P4 showed a peak, which is more noticeable in the profile of section P4. Liquid phase turbulence pattern is influenced by both the amount of sand deposited and the pipe bend. The

bend in the pipe increases the turbulence, while the turbulence is suppressed by the deposition of sand. Thus the profiles of turbulence kinetic energy at different sections show a complex patterns.

The mobility of the sand phase at the bottom-wall region of the bend pipe is an essential factor that indicated the various sand transport flow regimes in the pipe. Savage [40], Johnson and Jackson [34] and Bagnold [41] have previously demonstrated in their studies the relationship between solid particles stresses and the total normal stresses to the mobility of cohesion-less solid particles in fluids. In the present study, the rate of the sand mobility is evaluated as proportional to the ratio of the sand phase stresses, which include the particles translational and collisional stresses to the total normal stresses in the pipe, denoted **R**. The frictional component of the inter-particles interactions dissipated the sand and liquid phase shear stress and contributed to the total normal stress at certain conditions in the pipe when sand particles cluster may roll, maintain sliding enduring contacts or become stationary on the pipe bottom wall. It should be noted that the frictional component of the inter-particles interactions of the sand phase would be dominant when **R**=0. Observation of various solid transport regime would be explained with the predicted values of R in combination of solid concentration profiles presented in Figure 3.

Figures 9-11 present the curves of the evaluated ratio of the predicted translational-collisional stresses to the total normal stress for the sand

and liquid phase, at the various bend pipe sections at velocities above 1.5 m/s.

It is observed from the curves that at 3.7 m/s the ratio $\mathbf{R}$ is nonzero at the pipe bottom at all the pipe sections, P1-P4, particularly at section P3 where, $\mathbf{R} > 0.2$, as can be seen in the Figure 9. However, in the curve of section P2, which represents the pipe dip, $\mathbf{R}$ is close to zero at the pipe bottom wall. The point of vanishing shear stress, where $\mathbf{R} \to 0$ in the curves corresponds to the transition point below which collisional and friction stresses due to enduring contact between sand particles may coexist simultaneously in the pipe. The shear stress vanishing point in Figure 9 is located well close to the pipe bottom wall region, $^{y}/_{D} < 0.1$, of the bend pipe at the 3.7 m/s, particularly at sections P3 and P4. The near-uniformity of curves of the sand and liquid phase across the pipe indicated that most of the load in the pipe at 3.7 m/s is mainly carried by the liquid turbulence energy and the sand particles translational-collisional interactions mechanisms. The mobility of the sand phase at all the pipe sections at the 3.7 m/s is confirmed by the profiles of sand concentration in Figure 3, in which the sand concentration at the pipe bottom of the pipe sections is well below the loose-packed limit at 3.7 m/s. From the features of the curves in Figure 9 and the predicted sand concentration at the pipe bottom in Figure 3, the sand transport flow regime at the 3.7 m/s can be described as heterogeneous sand suspension in the majority of the bend pipe sections.

Figure 10 presents the curves of the **R** at the various bend pipe sections at 3 m/s velocity. It is observed from Figure 10 that the **R**-value at

sections P2 and P4 is zero at the pipe bottom region ${}^{y}/_{D} < 0.1$, but those of sections P1 and P3 are nearly zero and non-zero ($\mathbf{R} > 0.05$), respectively. The $\mathbf{R} = 0$ observed at the pipe bottom region ${}^{y}/_{D} \leq 0.1$ at sections P1 and P4 indicated that the sand-phase is immobile at the bottom of bend pipe sections at the 3 m/s velocity. It should be noted that the critical condition that identifies the minimum transport velocity to avoid sand deposit at the pipe bottom is that in which $\mathbf{R} = 0$ at ${}^{y}/_{D}$ =0 (pipe bottom-wall). The critical velocity corresponds to the condition at the onset of non-shearing sand particles and formation of enduring contact sand-particles clusters at the pipe bottom wall, ${}^{y}/_{D}$ =0. The sand-particles clusters may roll, agglomerate to form moving or stationary sand bed, depending on the degree of compaction of the sand particles in the bed which mainly depends on the thickness of the non-shearing zone, where $\mathbf{R} = 0$ in the pipe region $0 < {}^{y}/_{D} < 1$ and the interstitial liquid-phase shear stress in the non-shearing region.

The concentration of sand at the pipe bottom of the pipe sections at 3 m/s observed in Figure 3 and the features of the curves of the pipe sections in Figure 10 indicated that various sand transport regimes existed in the ±6° bend pipe simultaneously at 3 m/s velocity. It should be noted that the critical features of the curves mentioned include the **R**-value, the non-shearing zone thickness and near-uniformity of the curves. At sections P1 and P3, the curves indicated heterogeneous sand suspension and rolling sand-deposit regimes, respectively, whereas those of sections P2 and P4 indicated stationary and moving sand bed regimes, respectively.

The features of the curves of **R** at 2.5 m/s as can be seen in Figure 11 and the profiles of sand concentration in Figure 3 indicated that the sand phase is heterogeneously suspended at section P3 of the bend pipe, whereas stationary sand bed existed at sections P2 and P4 of the bend pipe.

In addition, it is observed that the liquid phase **R**-value is non-zero at certain region where, $^{y}/_{D} < 0.07$, in which the sand phase is non-shearing at section P2, as can be seen in Figure 11. This observation indicated that certain layer of the stationary sand bed thickness at section P2 is mobile, which can be described as a moving bed layer on a stationary bed layer at the pipe bottom wall at 2.5 m/s.

The various sand transport flow regimes observed at 3m/s and 2.5 m/s velocities from the profiles of sand concentration in Figure 3 and the curves of **R** in Figures 10-11 indicated that immobile sand bed already existed in the bend pipe at the velocities above the 1.5 m/s MTV estimated for an equivalent horizontal pipe. The immobile sand bed is significant at sections P2 and P4 of the bend pipe.

Figures 12 and 13 present curves of **R** at 1.5 m/s and 1 m/s, velocities at the MTV estimated for horizontal pipe and below, respectively. It is observed that the **R**=0 in the pipe bottom region, $^{y}/_{D} \leq 0.15$ at all the pipe sections at the velocities of 1.5 m/s and 1 m/s. The **R**-value is also zero at the pipe dip-exit, section-P3 where the liquid turbulence intensity has

been observed to be favoured by the perturbation in the flow between section P2 and P3. This observation indicated that the sand-phase is immobile in the entire bend pipe bottom region at the 1.5 m/s and 1 m/s. The thickness of the region where the **R**=0 varies at the various pipe sections. The various thickness of the immobile sand zone indicated that moving and stationary sand beds of various thicknesses existed in the majority of the bend pipe sections, particularly at sections P1 and P4.

It is observed that the near-uniformity of the curves is reduced as the thickness of the zone where particle frictional interactions increased, as evident in Figure 13. The interstitial liquid in the stationary sand bed region is stagnant as indicated by the **R**=0 for the liquid phase at the pipe bottom region. This observation indicated that the contributions of the liquid turbulence and the sand-phase translational-collisional stresses have reduced significantly at 1 m/s. The condition in the $\pm 6^{o}$ bend pipe may be described as partial pipe blockage at the velocity range of 1.5 m/s and 1 m/s, considering the sand concentration at the pipe bottom in Figure 3 and the features of the curves of **R** at 1.5 and 1 m/s in Figures 12 and 13.

The stationary sand-bed flow regime is considered the most undesirable and severe flow regime that can impede fluid flow in pipelines. Therefore, it is considered important to examine all the possible modes of occurrence of immobile sand deposit in the pipe bend sections P1-P4. The modes include whether or not the sand-phase is stationary at a section, or at multiple sections of the pipe bend under a certain operating condition. The possible

modes have been determined by the concept of factorial design of experimental, in which certain factors are used to determine the possible scenarios in a single experiment in order to examine all possible outcomes. The pipe sections P1, P2, P3 and P4 are the independent components in the present case, while the levels of possibilities of the presence of immobile sand phase in any of the pipe sections are defined by 'Yes' or 'No', which is determined by the R-value at region, $^{y}/_{D} = 0.05$ of the $\pm 6^{o}$ and $\pm 4^{o}$ V-inclined pipe bends. Therefore, the present case has four factors and two levels, which resulted to $2^4 = 16$ possible conditions of stationary sand deposit in the pipe bend. Tables 2 and 3 present the possible stationary sand bed conditions in $\pm 6^{o}$and $\pm 4^{o}$ pipe bends, respectively.

Although the design of experiment suggested that 16 possible conditions of stationary sand deposit formation may occur in the pipe bend sections, the CFD simulation results show that 6 of the conditions (condition code 1, 2, 4, 7, 12, 16) have been observed in the $\pm 6^{o}$ pipe bend and 7 conditions (condition code 1, 2, 4, 7, 8, 12, 16) in the $\pm 4^{o}$ pipe bend investigated, as can be seen in Tables 2 and 3, respectively. The Tables show that the critical transport velocity to ensure complete sand transport without sand deposit in the 6^{O} pipe bend is 3 m/s, but the velocity may be as low as 2.5 m/s for the $\pm 4^{o}$ pipe bend. The effect of the pipe curvature on the sand deposition in the pipe is revealed by the condition code-8, which represents the presence of stationary deposit in the downward, dip and dip-exit of the pipe bend. The condition is observed in the $\pm 4^{o}$ pipe bend, but not observed in the $\pm 6^{o}$ pipe bend. This observation indicates that the turbulence energy at the dip-exit, P3, is enhanced with the increase in

pipe bend angle and is the increased turbulence keeps sand in suspension longer at the dip-exit of the $\pm 6^{o}$ pipe bend compared to the $\pm 4^{o}$ pipe bend. The condition code-16 which represents the presence of stationary sand deposit in the entire pipe bend is the most critical condition. The pipe may be described as completely plugged by sand deposit at the condition code-16. This condition will occur in the pipe bends when the flow velocity is $\leq$ 1.2 m/s.

4. Conclusions

A 3D computational fluid dynamics (CFD) model has been developed in Eulerian-Eulerian methodology with kinetic theory of granular flow to investigate sand transport in turbulent pipe flow. The CFD model takes into account the co-existence of inter-particle collisional-frictional interactions to represent the intermediate-heterogeneous conditions of solids transport flow regime. The following important conclusions have been drawn from the present study:

1. The sand transport characteristics and MTV are strongly dependent on the seemingly small V-inclined bend pipes investigated. The results show that slight bend pipe curvatures of subsea petroleum pipelines may cause partial pipe blockage in certain sections of the pipelines at relatively high velocity due to formation of unexpected stationary sand deposit at the vicinity of pipe dips. The shear stress analysis provides a quantitative criterion for identification of stationary sand deposit formation and estimation of obstructive sand bed height at the bottom of pipes.

2. The correlations for predicting minimum sand transport velocity (MTV) developed based on data obtained from horizontal pipe and other forms of inclined pipe may be inaccurate for predicting the limit sand deposit velocity in V-inclined bend pipe sections. The threshold velocity to keep sand entrained in liquid in V-inclined bend pipe is significantly higher than that for horizontal pipes. Therefore, it is important for researchers and operators of petroleum pipelines to know the limitations of a correlation used for the solids MTV predictions.

3. The importance of having an accurate MTV correlation for solids transport in low angle pipe bends is evident in the mode of stationary sand formation predicted. It can be said that the critical sand transport velocity that prevents stationary sand deposit in horizontal pipe may be that at which plugged pipe condition may exist in pipe bend sections of undulating pipelines. Therefore, a predetermined critical sand transport velocity in which the effect of the pipe bends section has been incorporated will enable unhindered flow through pipe bend sections and the entire sections of long undulating pipelines such as subsea petroleum pipelines.

Funding

This research did not receive any specific grant from funding agencies in the public, commercial, or not-for-profit sectors.

References

1. DABIRIAN, R., MOHAN, R.S., SHOHAM, O. and KOUBA, G., 2015, September. Sand Transport in Stratified Flow in a Horizontal Pipeline. In *SPE Annual Technical Conference and Exhibition*. Society of Petroleum Engineers.

2. SPILLANE, C., and LEGGOE, J., 2011. Investigation into sand deposition of transportation in multiphase pipelines. *Proceedings of the CEED Seminar 2011*. pp. 13-18.

3. BELLO, K. O., OYENEYIN, M. B. and OLUYEMI, G. O., 2011. Minimum transport velocity models for suspended particles in multiphase flow revisited. *Proceeding of the Society of Petroleum Engineers Annual Technical Conference and Exhibition SPE 147045*. 30 October -2 November 2011. Denver, Colorado. pp. 1-10.

4. ZHU, Z., SAND, K.W., and TEEVENS, P.J., 2010. Solids deposition in liquids petroleum (oil) and wet-gas pipelines for internal corrosion predictive modelling (ICPM). *Nace International*

5. LONDON, M., CAMERON, S., and PIERCE, G. Flow loop for x-ray ct imaging of sand transport. *Proceedings of the SPE Heavy Oil Conference*. SPE 157897. Alberta. 12-14 June 2012. pp. 1-15.

6. GUZMAN, J. E. V. and ZENIT, R., 2011. Application of the euler-lagrange method to model developed hydrodynamic slugs in conduits. *Journal of fluids engineering,* 133, pp. 1-9.

7. SOEPYAN, F. B. et al., 2014. Solids transport models comparison and fine-tuning for horizontal low concentration flow in single-phase carrier fluid. *America Institute of Chemical Engineers Journal*, 60 (1), pp. 76-121.

8. DANIELSON, T. J., 2007. Sand transport modelling in multiphase pipelines. *Proceedings of the Offshore Technology Conference, OTC 18691.* 30 April-3 May 2007. Houston, Texas. pp. 1-11.

9. DE HENAU, V. and RAITHBY, G.D., 1995. A study of terrain-induced slugging in two-phase flow pipelines. *International journal of multiphase flow*, *21*(3), pp.365-379.

10. AL-LABABIDI, S., YAN, W., and YEUNG, H., 2012. Sand transportations and deposition characteristics in multiphase flows in pipelines. *Journal of Energy Resources Technology*. 134, pp. 1-13.

11. DOAN, Q., et al., 1996. Simulation of sand transport in a horizontal well. *Proceedings of the SPE International Conference on Horizontal Well Technology*. SPE 37106. 18-20 November. pp. 581-593.

12. OUDEMAN, P., 1992. Sand transport and deposition in horizontal multiphase trunklines of subsea satellite developments. *Proceedings of the Offshore Technology Conference, OTC 7059*. 4-7 May 1992. Houston, Texas. pp. 659-667.

13. SALAMA, M. M., 2000. Influence of sand production on design and operation of piping systems. *Corrosion2000. Proceedings of the NACE International Conference*. Houston, Texas. Paper No. 00080.

14. DORON, P. and BARNEA, D., 1995. Pressure drop and limit deposit velocity for solid-liquid flow in pipes. *Chemical Engineering Science*, 50(10), pp. 1595-1604.

15. OSHO, A.J., YAN, W., and YEUNG, H., 2012. Experimental study of air-water flow in undulating pipeline and implication on sand transport. *Offshore Technology Conference, OTC 23331*. 30 April-3 May. Houston, Texas, USA.

16. YAN, W., HU, X. Osho, Y and YEUNG, H., 2011. Experimental study on sand transport characteristics in water and air-water flow in dip pipeline. *BHR Group Multiphase* 15, pp. 51-68.

17. KING, M. J. S., FAIRHURST, C. P., and HILL, T. J., 2001. Solids transport in multiphase flows-application to high viscosity systems. *American Society of Mechanical Engineers ASME*, 123, pp. 200-204.

18. TIPPET, J. R. and PRIESTMAN, G. H., 1997. Mobility of solids in multiphase undulating pipeline. *In: A. P. BURNS, ed. how deep? how far? how soon? Proceedings of the 8th International Conference on Multiphase 1997.* Vol. 24. London. Mechanical Engineering. pp. 125-132.

19. ZHENG, G., BRLL, J. P., and SHOHAM, O., 1993. Hilly terrain effects on slug flow characteristics. *Proceedings of the 68th Annual Technical Conference and Exhibition of the Society of Petroleum Engineers. SPE 26566*. Houston, Texas, 3-8 October 1993. pp. 529-541.

20. HUANG, S., ZHANG, B., LU, J. and WANG, D., 2013. Study on flow pattern maps in hilly-terrain air–water–oil three-phase flows. *Experimental Thermal and Fluid Science*, *47*, pp.158-171.

21. AL-SAFRAN, E. et al 2005. Investigation of slug flow characteristics in the valley of a hilly-terrain pipeline. *International Journal of Multphase Flow*, 31(3), pp. 337-357.

22. ISSA, R. I., and KWEMF, M. H. W., 2003. Simulation of slug flow in horizontal and nearly horizontal pipes with the two-fluid model. *International Journal of Multiphase Flow*, 29, pp. 69-95.

23. TAITEL, Y., SARICA, C. and BRILL, J.P., 2000. Slug flow modelling for downward inclined pipe flow: theoretical considerations. *International Journal of Multiphase Flow*, *26*(5), pp. 833-844.

24. GOHARZADEH, A., RODGERS, P. and WANG, L., 2013. Experimental Characterization of Slug Flow on Solid Particle Transport in a 1 Deg Upward Inclined Pipeline. *Journal of Fluids Engineering*, *135*(8), p. 081304.

25. NOSSAIR, A.M., RODGERS, P. and GOHARZADEH, A., 2012, November. Influence of Pipeline Inclination on Hydraulic Conveying of Sand Particles. In *ASME 2012 International Mechanical Engineering Congress and Exposition* pp. 2287-2293.

26. STEVENSON, P. and THORPE, R. B., 1999. Towards understanding sand transport in subsea flowlines. *In: A. P. BURNS, ed. frontier technology comes of age. Proceedings of the 9th International Conference on Multiphase 1999*. Vol. 35. Bury St Edmunds. Professional Engineering Publications. pp. 583-594.

27. KESENA, N. R. et al., 2014. Experimental study of sand particle concentration profiles in straight and pipe elbow for horizontal and pipe elbow for horizontal multiphase flows. *Journal of Energy Resources Technology*, 136, pp. 1-11.

28. AMIRI, A., ØYE, G., & SJÖBLOM, J, 2009. Influence of pH, high salinity and particle concentration on stability and rheological properties of aqueous suspensions of fumed silica. *Colloids and Surfaces A: Physicochemical and Engineering Aspects*, 349(1), pp. 43-54.

29. AMIRI, A., NULAND, S., ØYE, G., and SJÖBLOM, J., 2012. Use of a Cross-Sectional Model for Determining Rheology in Settling Slurries: Effect of Solvent, Particle Size, and Density. *Journal of Dispersion Science and Technology,* 33(9), pp. 1336-1345.

30. LUN, C.K.K., SAVAGE, S.B., JEFFREY, D.J. and CHEPURNIY, N., 1984. Kinetic theories for granular flow: inelastic particles in Couette flow and slightly inelastic particles in a general flowfield. Journal of fluid mechanics, 140, pp. 223-256.

31. GIDASPOW, D., BEZBURAH, R. and DING, J. Hydrodynamics of Circulating Fluidized Beds, Kinetic Theory Approach. In Fluidization VII, the 7th Engineering Foundation Conference on Fluidization (ed O.E. Potter and D. J. Nicklin), Brisbane, Australia, 3-8 May 1992, pp. 75–82.

32. SYAMLAL, M., ROGERS, W. and O'BRIEN, T.J., 1993. MFIX documentation: Theory guide. National Energy Technology Laboratory, Department of Energy, Technical Note DOE/METC-95/1013 and NTIS/DE95000031.

33. SCHAEFFER, D.G., 1987. Instability in the evolution equations describing incompressible granular flow. Journal of differential equations, 66(1), pp. 19-50.

34. JOHNSON, P.C. AND JACKSON, R., 1987. Frictional–collisional constitutive relations for granular materials, with application to plane shearing. *Journal of Fluid Mechanics*, 176, pp.67-93.

35. Fluent Theory Guide, Version 14.0, 2011.

36. EKAMBARA, K., SANDERS, R.S., NANDAKUMAR, K. and MASLIYAH, J.H., 2009. Hydrodynamic simulation of horizontal slurry pipeline flow using ANSYS-CFX. Industrial & Engineering Chemistry Research, 48(17), pp.8159-8171.

37. KAUSHAL, D. R., and TOMITA, Y., 2013. Prediction of concentration distribution in pipeline flow of highly concentrated slurry. *Particulate Science and Technology: An International Journal*, 31(1), pp. 28-34.

38. OROSKAR, A. R., and TURIAN, R. M., 1980. The critical velocity in pipeline flow of slurries. American Institute of Chemical Engineers Journal, 26(4), pp. 55-558.

39. SAVAGE, S.B., 1984. The mechanics of rapid granular flows. *Advances in applied mechanics*, 24, pp. 289-366.

40. BAGNOLD, R.A., 1956. The flow of cohesionless grains in fluids. *Philosophical Transactions of the Royal Society of London A: Mathematical, Physical and Engineering Sciences*, *249*(964), pp.235-297.

Nomenclature

Symbol	**Description**	**Unit**
C_D	Drag coefficient	-
C_v	Solids volume fraction	-
D	Pipe diameter (size)	m
$D_{t,sl}$	Turbulent quantities for solids phase	-
d_s	Particle diameter (size)	m

e_{ss}	Coefficient of restitution of particles	-
ε	Turbulence dissipation rate	m^2s^{-2}
F_D	Drag force	N
F_{td}	Turbulent dispersion force	N
F_{vm}	Virtual mass force	N
g	Gravitational constant	ms^{-2}
$g_{0,ss}$	Radial distribution function	-
I_{2D}	Second invariant of the deviator of the strain	-
k_l	Turbulent kinetic energy of liquid phase	m^2s^{-2}
k_{ls}	Covariance of velocities of liquid and solids	m^2s^{-2}
k_s	Turbulent kinetic energy of solids phase	m^2s^{-2}
M_{ls}	Interfacial momentum transfer	Ns^{-1}
Pr	Prandtl number	-
P_{sf}	Solids frictional pressure	Nm^{-2}
P_s	Solids pressure	Nm^{-2}
R	Ratio of liquid and solids phase stress	-
Re	Reynolds number	-
U^*	Normalised velocity magnitude	-
v_l	Velocity of liquid phase	ms^{-1}
v_s	Velocity of solids phase	ms^{-1}
y^*	Normalised height of near wall mesh node	-

Greek letters

Θ_s	granular temperature	m^2s^{-2}

$\mu_{s,col}$	solids collisional viscosity	Pa.s
$\mu_{s,kin}$	solids kinetic viscosity	Pa.s
$\mu_{s,fr}$	solids frictional viscosity	Pa.s
$\alpha_{s,min}$	minimum frictional volume fraction	-
$\alpha_{s,max}$	maximum packing fraction limit of solids	-
Π_{kl}, $\Pi_{\varepsilon l}$	Influence of solids phases on liquid phase	-
$\tau_{F,sl}$	Characteristic particle relaxation time	s
$\tau_{t,sl}$	Lagrangian time scale	s
α_l	volume fraction of liquid phase	-
α_s	volume fraction of solids phase	-
η_{sl}	the ratio of the two characteristic times	-
ρ_m	mixture density	kg/m^3
ρ_i	liquid density	kg/m^3
ρ_s	solids density	kg/m^3
λ_s	Solids phase bulk viscosity	Pa.s
τ_w	Wall shear stress	Nm^{-2}
$\bar{\bar{\tau}}_l$	Viscous stress tensor for liquid phase	Nm^{-2}
μ_l	molecular viscosity of liquid phase	Pa.s
$\mu_{t,l}$	liquid turbulent viscosity	Pa.s
$\mu_{t,m}$	mixture turbulent viscosity	Pa.s
γ_{Θ_s}	granular energy dissipation	$kgm^{-3}s^{-1}$
Φ	angle of internal friction	-
ϕ_{ls}	energy exchange between particles and liquid	$kgm^{-3}s^{-1}$

List of Figure Caption:

Figure 1: Schematic of V-inclined pipe bend (not to scale)

Figure 2: Hexahedral mesh structures of 3D bend pipes: (a) ±6^{o} V bend pipe (b) ±4^{o} V bend pipe (not to scale)

Figure 2: Profiles of predicted sand concentration in ±6^{o} V inclined pipe bend at velocity range of 3.7 m/s-0.3 m/s

Figure 3: Contour plots at 3 m/s flow velocity: (a) sand concentration (b) liquid velocity magnitude.

Figure 4: Contour plots at 2.5 m/s flow velocity: (a) sand concentration (b) liquid velocity magnitude.

Figure 6: Contour plots at 1.5 m/s flow velocity: (a) sand concentration (b) liquid velocity magnitude.

Figure 7: Contour plots at 1 m/s flow velocity: (a) sand concentration (b) liquid velocity magnitude.

Figure 8: Comparison of predicted profiles of multiphase turbulence kinetic energy at ±6^{o} bend pipe sections

Figure 9: Curves of ratio of predicted sand and liquid phase stresses to the total stress in ±6^{o} bend pipe sections at 3.7 m/s.

Figure 10: Curves of ratio of predicted sand and liquid phase stresses to the total stress in ±6^{o} bend pipe sections at 3 m/s.

Figure 11: Curves of ratio of predicted sand and liquid phase stresses to the total stress in ±6^{o} bend pipe sections at 2.5 m/s

Figure 12: Curves of ratio of predicted sand and liquid phase stresses to the total stress in ±6^{o} bend pipe sections at 1.5 m/s.

Figure 13: Curves of ratio of predicted sand and liquid phase stresses to the total stress in ±6^{o} bend pipe sections at 1 m/s.

Table 1: Simulation condition for flow in bend pipe

Parameters	Pipe inclination	
	±6° V-pipe	±4° V-pipe
Pipe diameter (m)	0.1	
Velocity range (ms^{-1})	3.7 - 0.3	
Liquid density (kgm_3^{-1})	998	
Liquid viscosity (pa.s)	0.001	
sand density (kgm_3^{-1})	2650	
Particle size (μm)	255	
Sand fraction	0.04	
MTV (ms^{-1}) estimated for 0.1m diameter horizontal pipe and 255 μm particle size	1.48	

Table 2: Matrix of conditions for stationary sand deposit formation in $\pm 6^{o}$ V-inclined Pipe bend

Condition code	$R = 0$ at $^{y}/_{D} = 0.05$ of the bend pipe				Velocity range (m/s)	Comment
	P1	**P2**	**P3**	**P4**		
1	No	No	No	No	3.7-3	Mobile sand phase throughout pipe bend
2	Yes	No	No	No	< 3-2.5	stationary sand deposit at the downhill section
3	No	Yes	No	No	-	Unobserved condition
4	Yes	Yes	No	No	< 3-2	Stationary sand deposit at the downhill and dip sections
5	No	No	Yes	No	-	Unobserved condition
6	Yes	No	Yes	No	-	Unobserved condition
7	No	Yes	Yes	No	< 0.3	Plugged pipe-dip
8	Yes	Yes	Yes	No	-	Unobserved condition
9	No	No	No	Yes	-	Unobserved condition
10	Yes	No	No	Yes	-	Unobserved condition
11	No	Yes	No	Yes	-	Unobserved condition
12	Yes	Yes	No	Yes	1.5	Mobile sand phase at the dip-exit towards upward inclined pipe bend section
13	No	No	Yes	Yes	-	Unobserved condition
14	Yes	No	Yes	Yes	-	Unobserved condition
15	No	Yes	Yes	Yes	-	Unobserved condition
16	Yes	Yes	Yes	Yes	1.2-0.3	Stationary sand deposit throughout the pip bend Plugged pipe condition

Table 3: Matrix of conditions for stationary sand deposit formation in $\pm 4^{o}$ V-inclined Pipe bend

Condition code	$R = 0$ at $^{y}/_{D} = 0.05$ of the bend pipe				Velocity range (m/s)	Comment
	P1	**P2**	**P3**	**P4**		
1	No	No	No	No	3.7-2.5	Mobile sand phase throughout pipe bend
2	Yes	No	No	No	2	stationary sand deposit at the downhill section
3	No	Yes	No	No	-	Unobserved condition
4	Yes	Yes	No	No	< 2-1.2	Stationary sand deposit at the downhill and dip sections
5	No	No	Yes	No	-	Unobserved condition
6	Yes	No	Yes	No	-	Unobserved condition
7	No	Yes	Yes	No	< 0.3	Plugged pipe-dip
8	Yes	Yes	Yes	No	1.2	Stationary deposit at the downward, dip and dip exit
9	No	No	No	Yes	-	Unobserved condition
10	Yes	No	No	Yes	-	Unobserved condition
11	No	Yes	No	Yes	-	Unobserved condition
12	Yes	Yes	No	Yes	1.5	Mobile sand phase at the dip-exit in upward inclined pipe bend section
13	No	No	Yes	Yes	-	Unobserved condition
14	Yes	No	Yes	Yes	-	Unobserved condition
15	No	Yes	Yes	Yes	-	Unobserved condition
16	Yes	Yes	Yes	Yes	1-0.3	Stationary sand deposit throughout the pip bend

						Plugged pipe condition

Figures

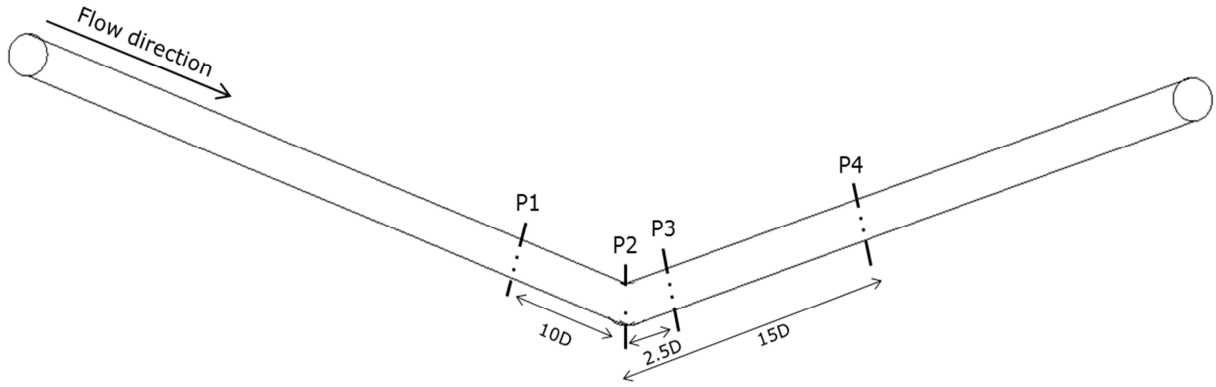

Figure 1: Schematic of V-inclined pipe bend (not to scale)

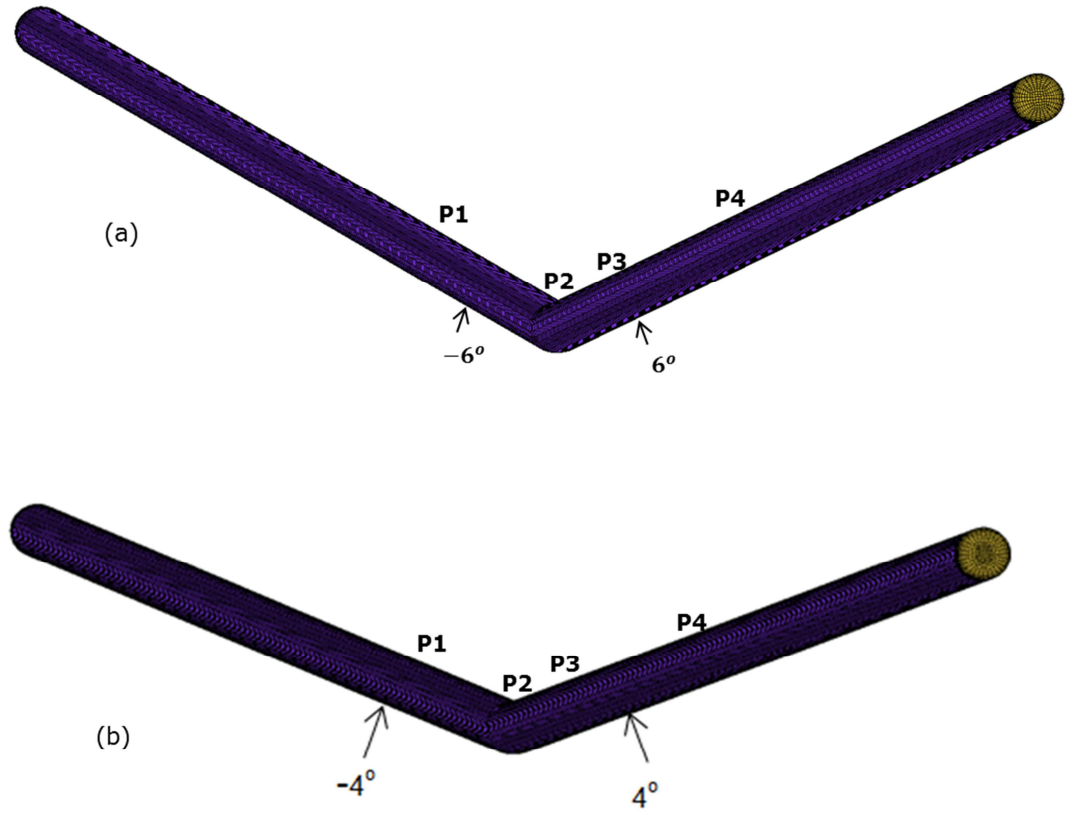

Figure 2: Hexahedral mesh structures of 3D bend pipes: (a) ±6° V bend pipe (b) ±4° V bend pipe (not to scale)

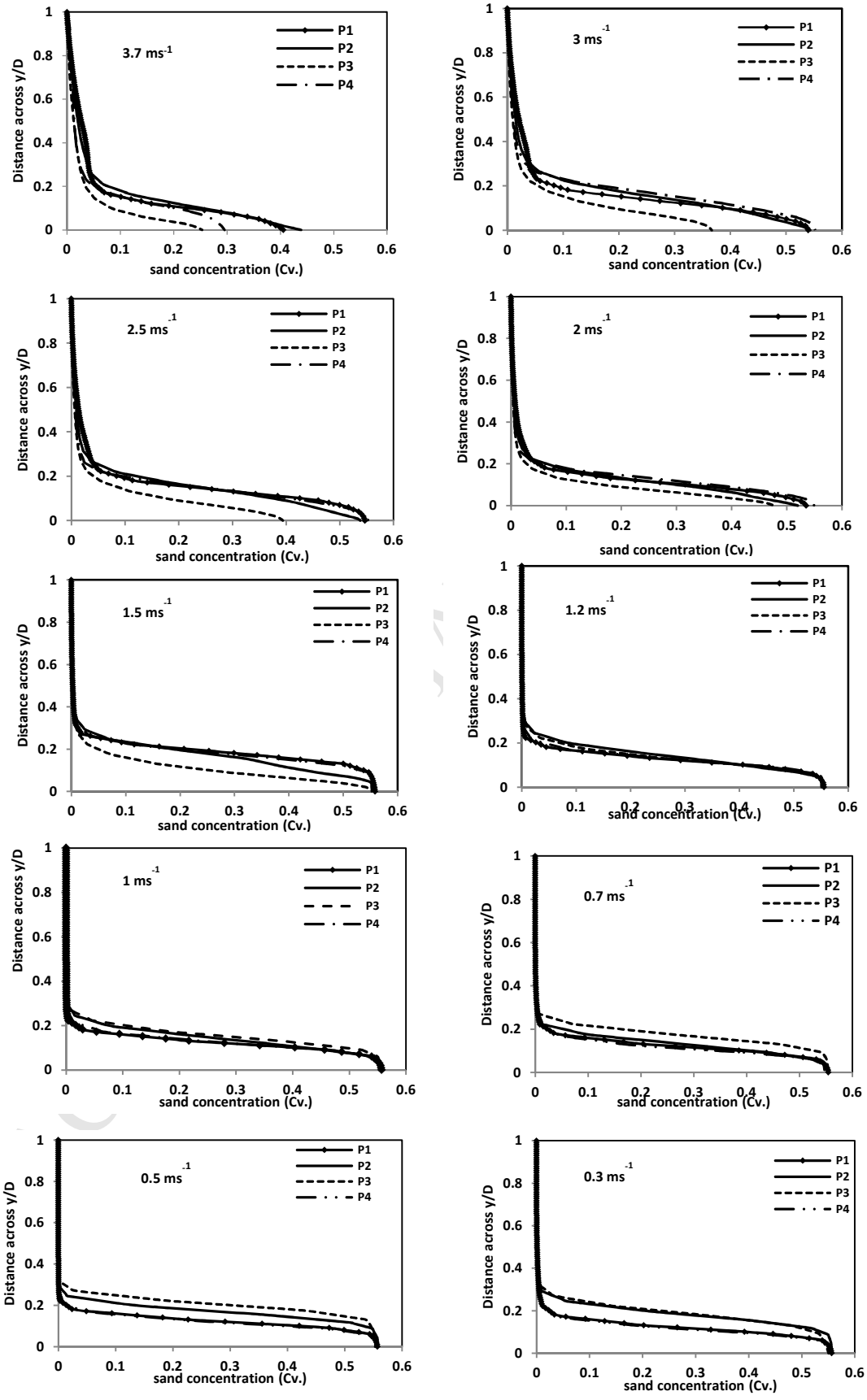

Figure 2: Profiles of predicted sand concentration in ±6° V inclined pipe bend at velocity range of 3.7 m/s-0.3 m/s

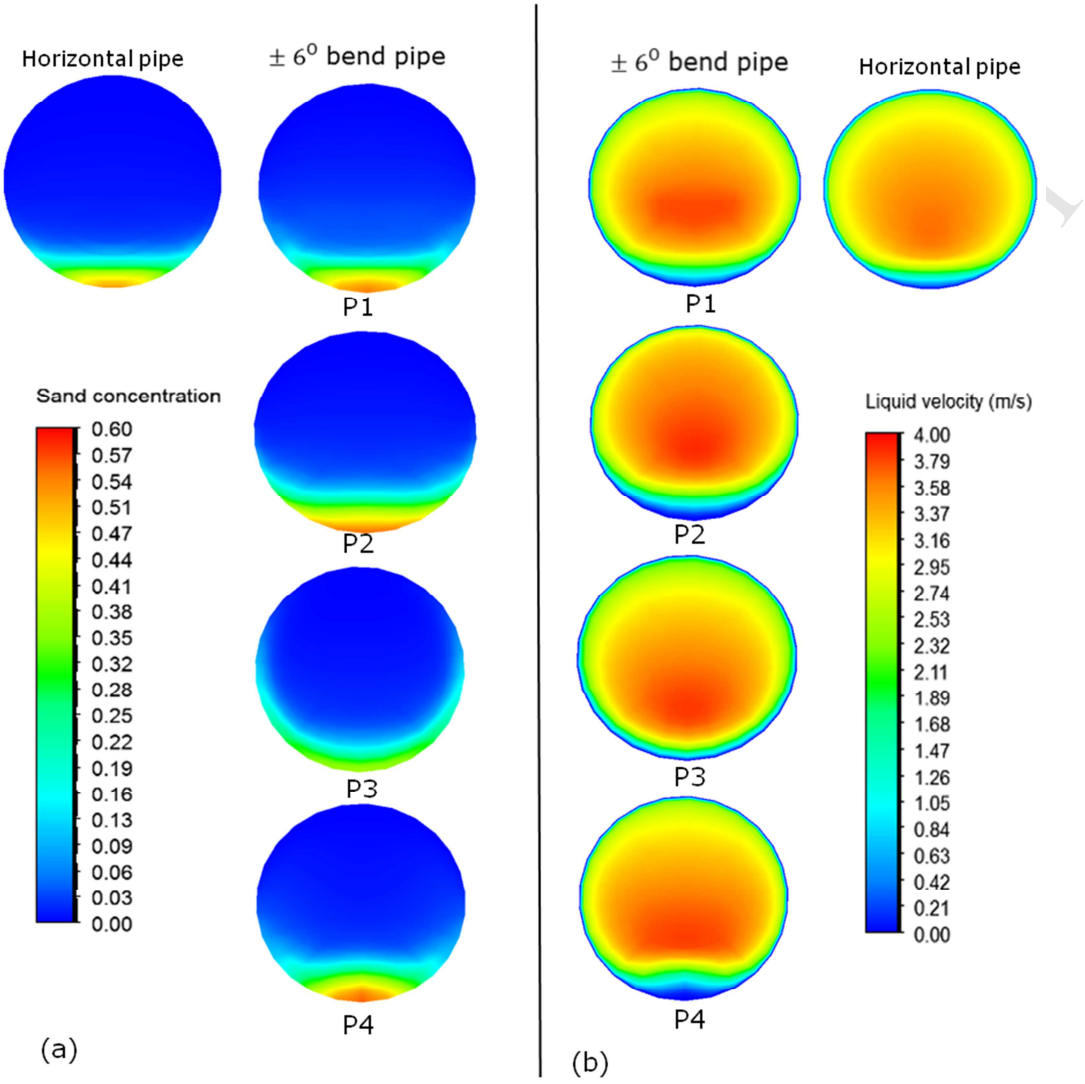

Figure 3: Contour plots at 3 m/s flow velocity: (a) sand concentration (b) liquid velocity magnitude.

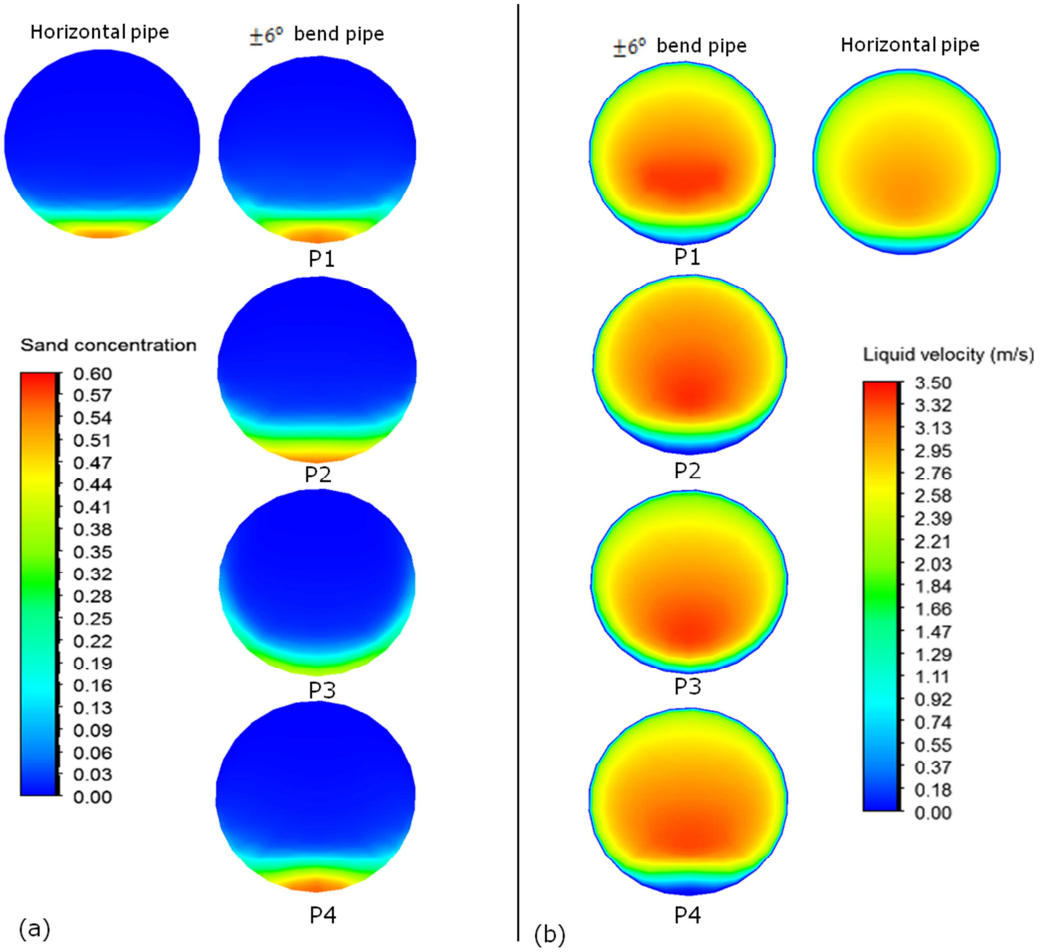

Figure 4: Contour plots at 2.5 m/s flow velocity: (a) sand concentration (b) liquid velocity magnitude.

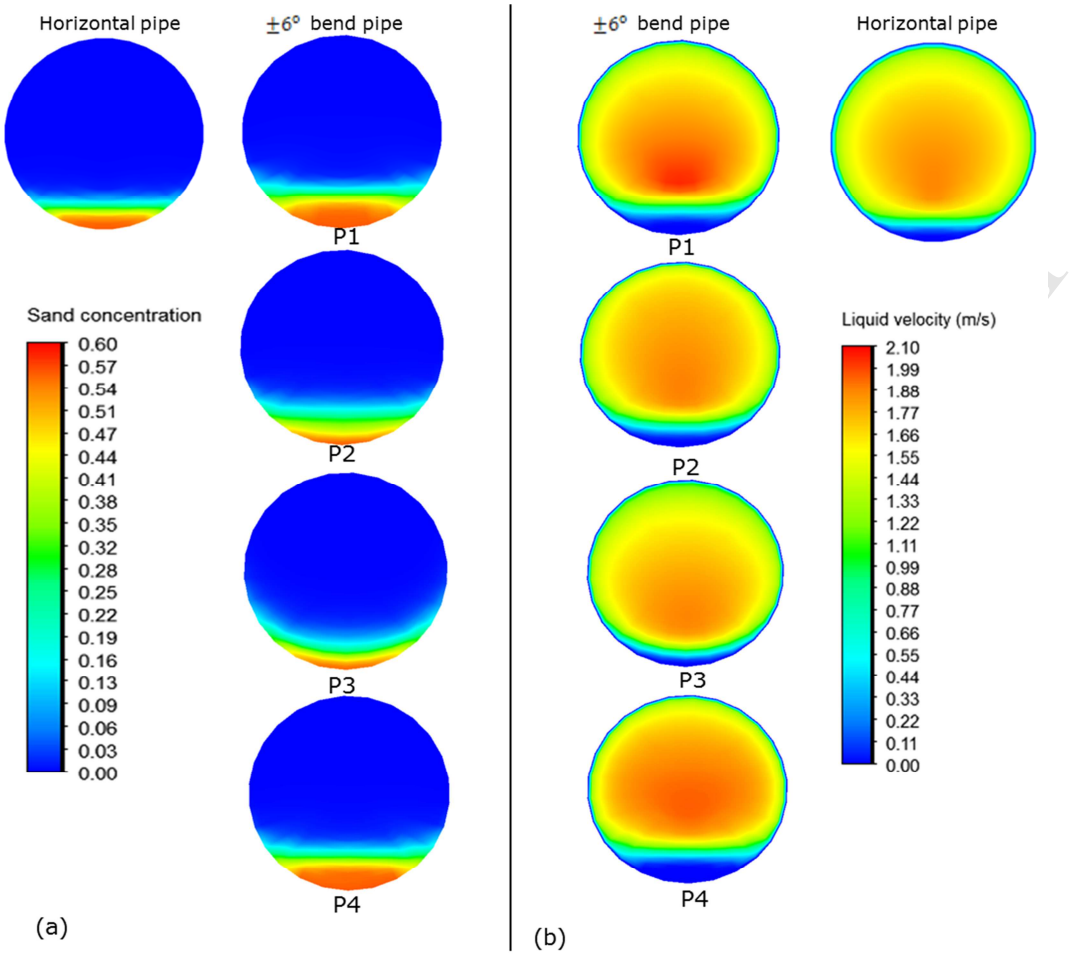

Figure 6: Contour plots at 1.5 m/s flow velocity: (a) sand concentration (b) liquid velocity magnitude.

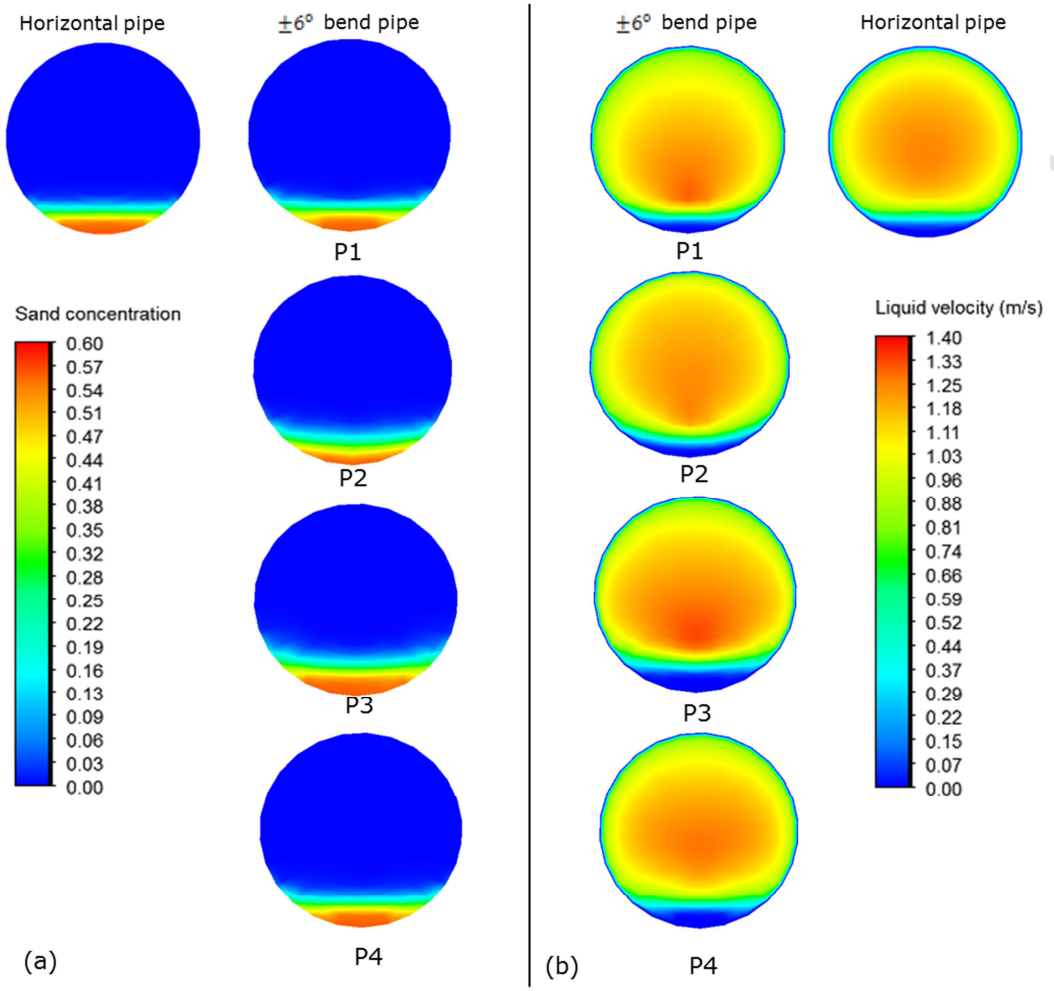

Figure 7: Contour plots at 1 m/s flow velocity: (a) sand concentration (b) liquid velocity magnitude.

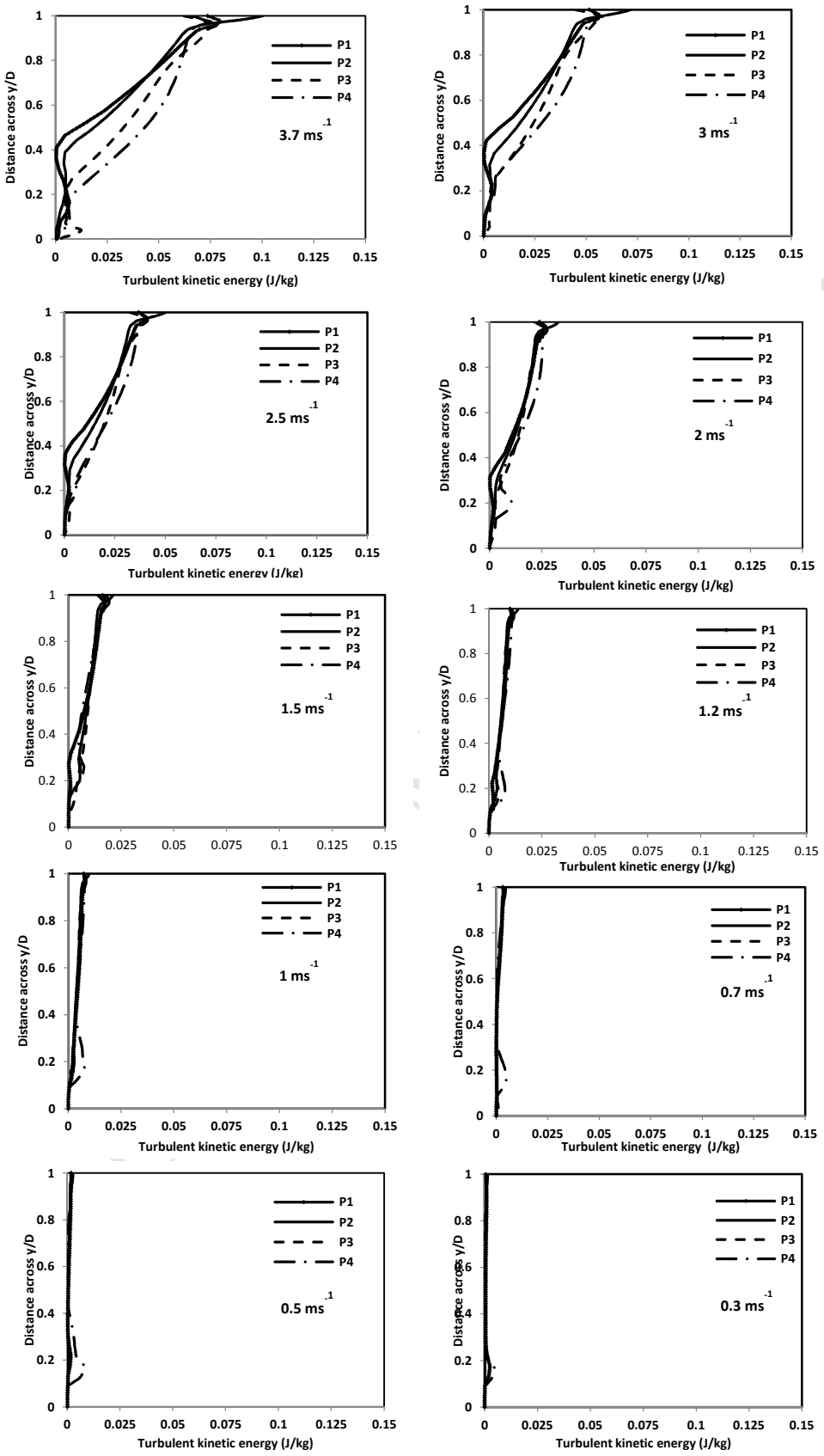

Figure 8: Comparison of predicted profiles of multiphase turbulence kinetic energy at ±6^{o} bend pipe sections

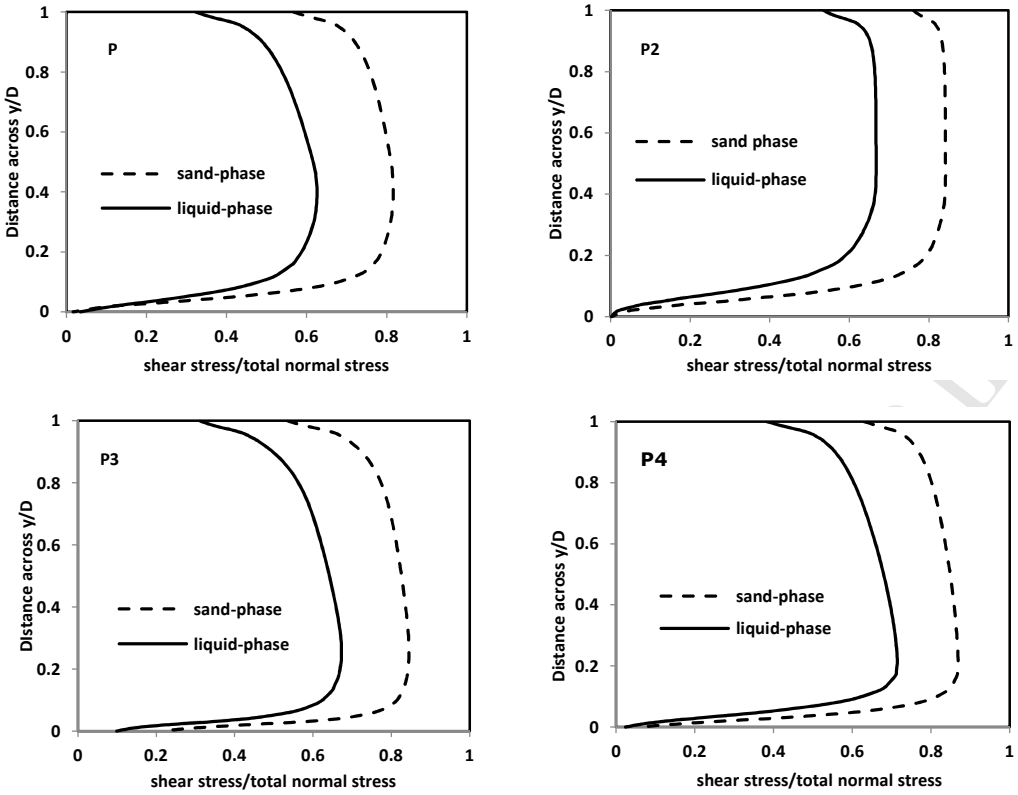

Figure 9: Curves of ratio of predicted sand and liquid phase stresses to the total stress in ±6° bend pipe sections at 3.7 m/s.

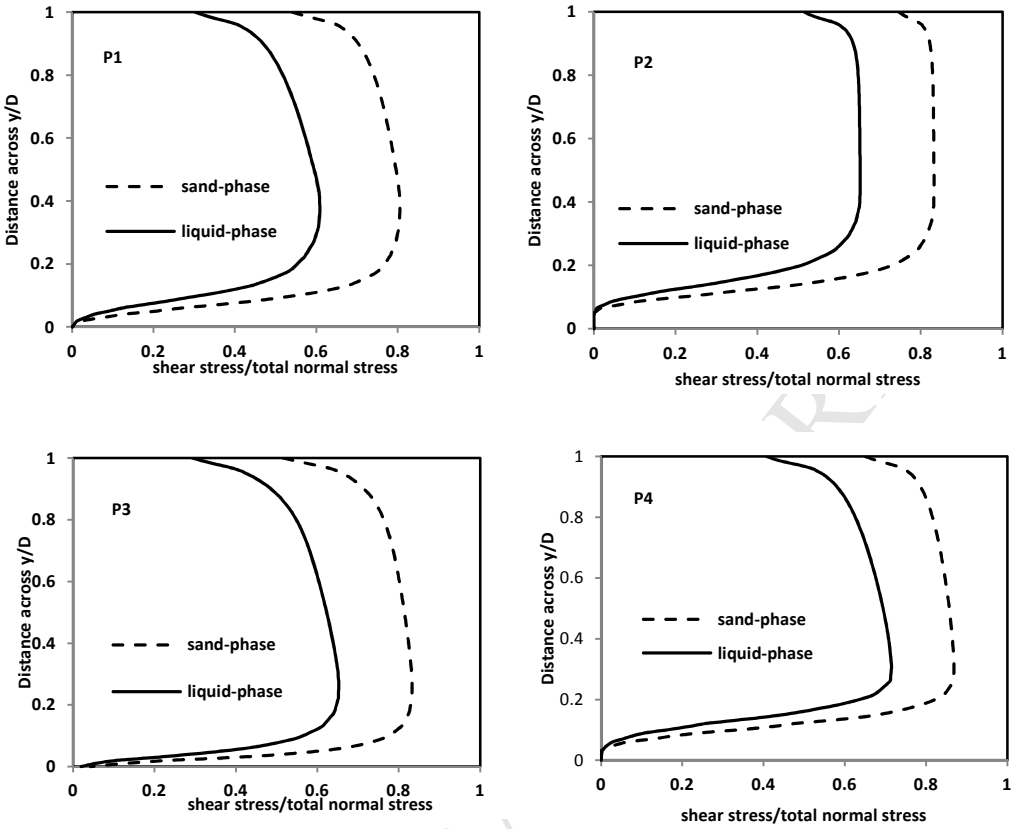

Figure 10: Curves of ratio of predicted sand and liquid phase stresses to the total stress in ±6° bend pipe sections at 3 m/s.

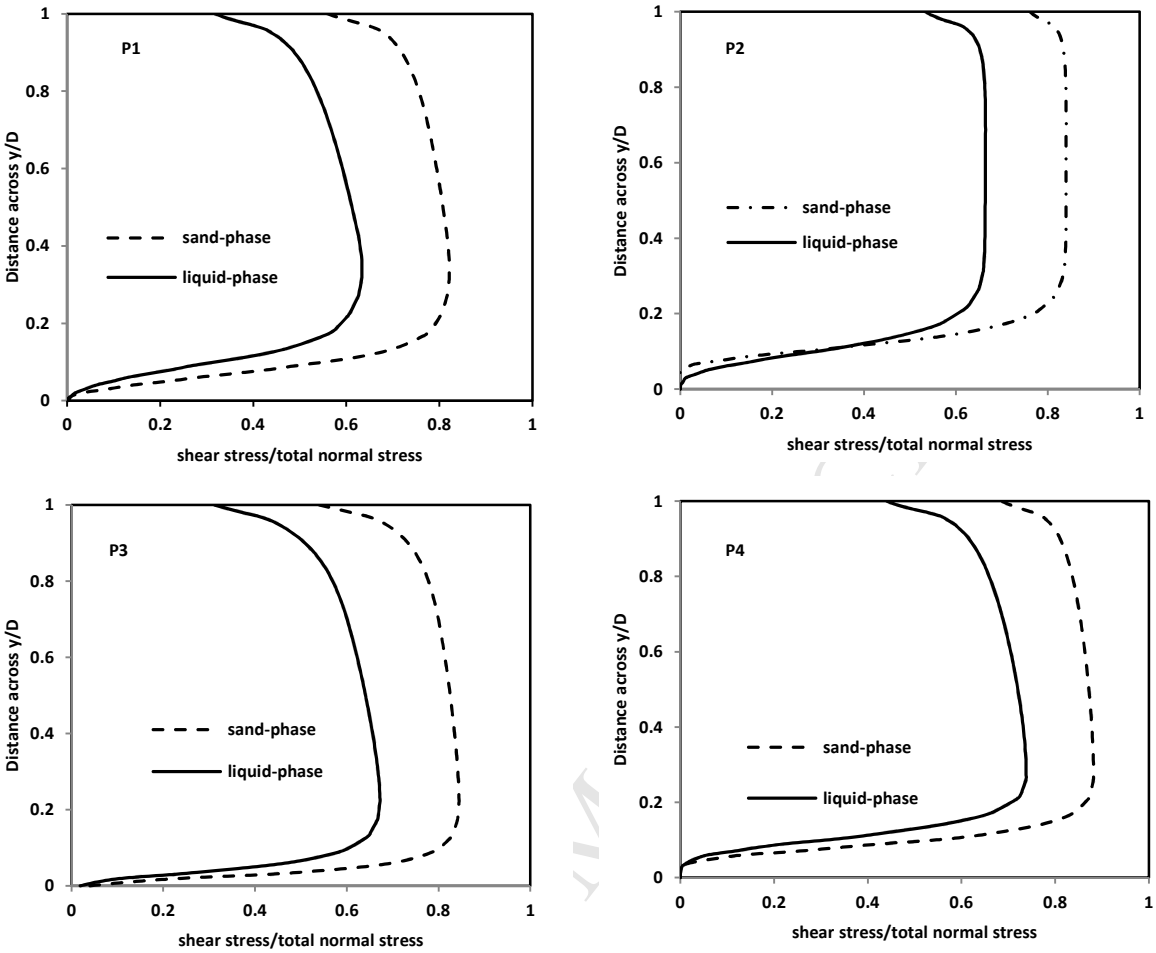

Figure 11: Curves of ratio of predicted sand and liquid phase stresses to the total stress in ±6° bend pipe sections at 2.5 m/s

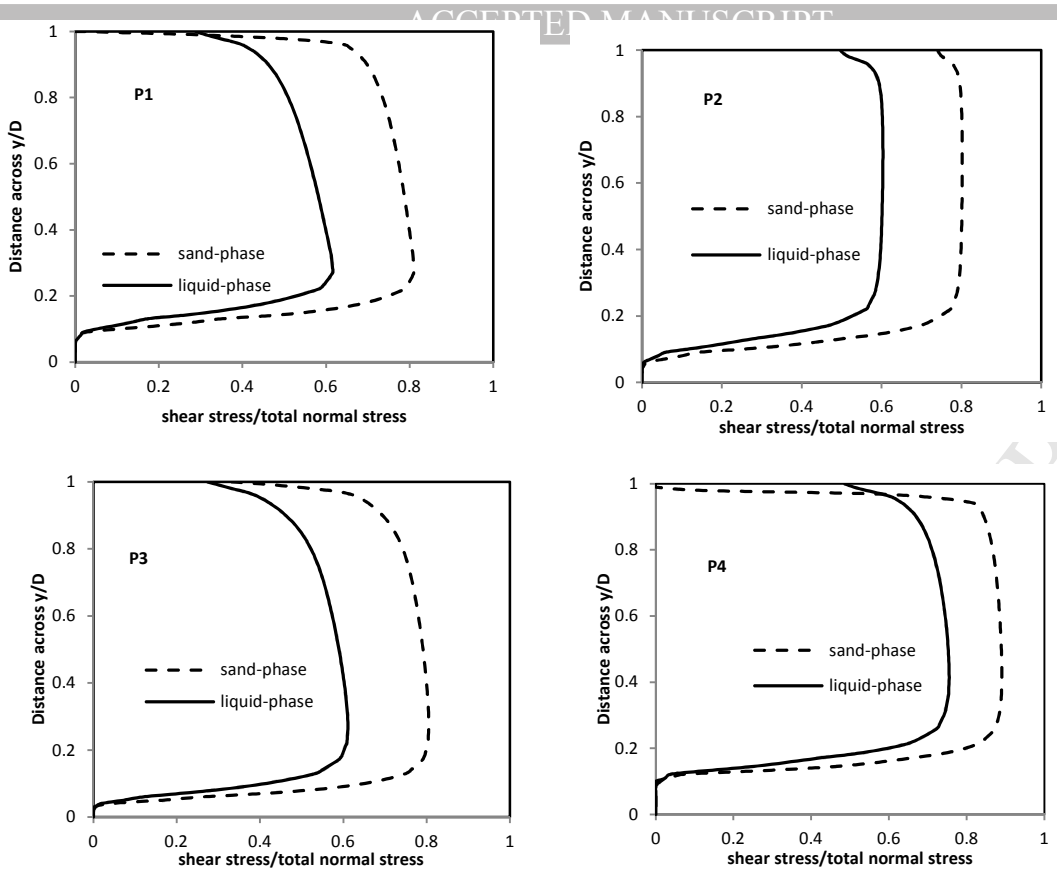

Figure 12: Curves of ratio of predicted sand and liquid phase stresses to the total stress in ±6° bend pipe sections at 1.5 m/s.

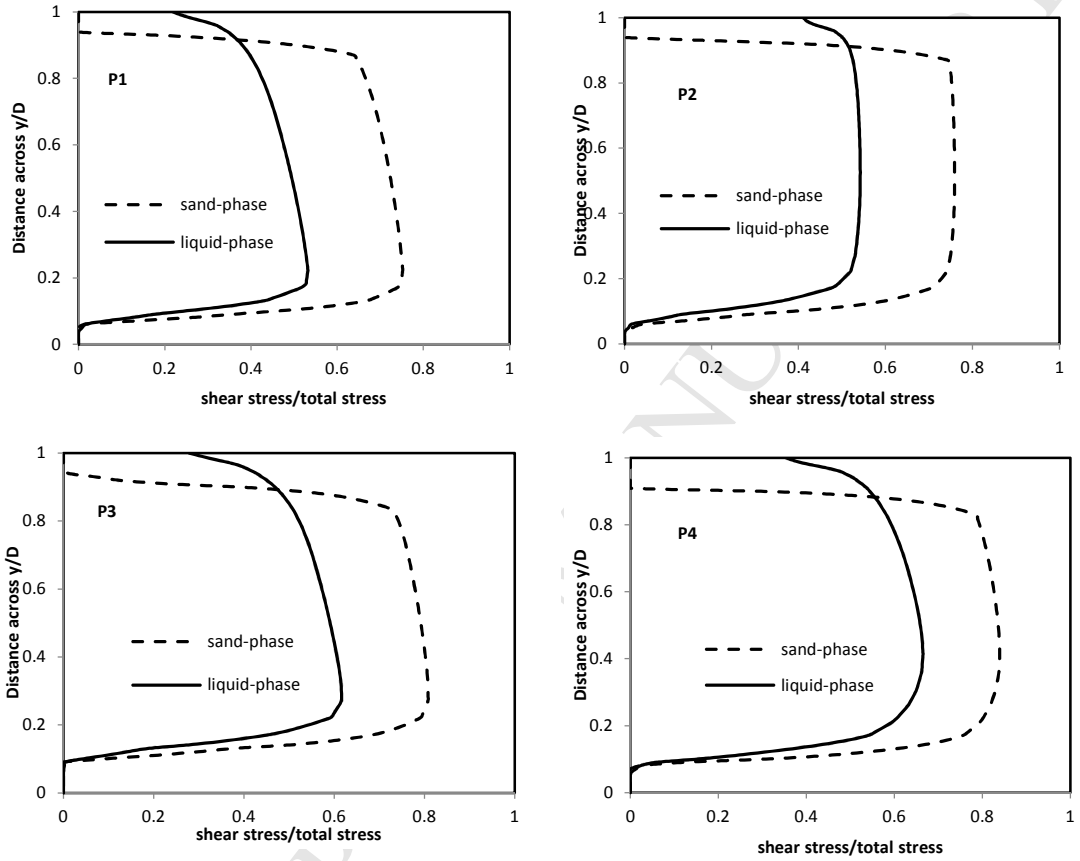

Figure 13: Curves of ratio of predicted sand and liquid phase stresses to the total stress in ±6° bend pipe sections at 1 m/s.

Highlights

Solid transport flow regime transition has been investigated computationally in undulated pipe
Small angled V-inclined pipe significantly altered the solid transport regime compared to a straight pipe
Solid deposition takes place at the downstream section of V-inclined pipe at much higher velocities